

Unraveling Polysulfide's Adsorption and Electrocatalytic Conversion on Metal Oxides for Li-S Batteries

Shungui Deng, Tiezhu Guo, Jakob Heier,* and Chuanfang (John) Zhang*

Lithium sulfur (Li-S) batteries possess high theoretical capacity and energy density, holding great promise for next generation electronics and electrical vehicles. However, the Li-S batteries development is hindered by the shuttle effect and sluggish conversion kinetics of lithium polysulfides (LiPSs). Designing highly polar materials such as metal oxides (MOs) with moderate adsorption and effective catalytic activity is essential to overcome the above issues. To design efficient MOs catalysts, it is critical and necessary to understand the adsorption mechanism and associated catalytic processes of LiPSs. However, most reviews still lack a comprehensive investigation of the basic mechanism and always ignore their in-depth relationship. In this review, a systematic analysis toward understanding the underlying adsorption and catalytic mechanism in Li-S chemistry as well as discussion of the typical works concerning MOs electrocatalysts are provided. Moreover, to improve the sluggish “adsorption-diffusion-conversion” process caused by the low conductive nature of MOs, oxygen vacancies and heterostructure engineering are elucidated as the two most effective strategies. The challenges and prospects of MOs electrocatalysts are also provided in the last section. The authors hope this review will provide instructive guidance to design effective catalyst materials and explore practical possibilities for the commercialization of Li-S batteries.

market for over 30 years, greatly impacting to the society and our daily lives. However, each energy storage technology is limited by its theoretical capacity. The quest for a “beyond Li-ion battery” system is thus ongoing.

Among the competitors in the high energy storage arena, lithium sulfur (Li-S) batteries emerged as a promising system with a high theoretical specific capacity of 1675 mAh g⁻¹ and potential energy density up to 2600 Wh kg⁻¹, which is more than 5 times of the value of Li-ion batteries. In addition with the substantially reduced costs and intrinsic environmental benignity of Li-S chemistry, these superiorities make Li-S chemistry an attractive candidate for the application in smart grid and EVs.^[1] Nevertheless, the development of Li-S batteries is hampered by a series of fundamental challenges. First, the inherently insulating nature of S₈ and reduced component Li₂S, with low conductivities of 5 × 10⁻³⁰ and 10⁻¹³ S cm⁻¹, respectively, impedes the transfer of electrons. As such, conductive additives are added to improve cathode electron conductivity. Second, the volume


change between S₈ and Li₂S is nearly 80%, where the volume strain leads to negative effects in the durability of Li-S batteries. Last but not most important, the soluble intermediate lithium polysulfides (LiPSs) dissolve in commonly used electrolytes and travel between cathode and anode driven by concentration diffusion, which is generally known as “shuttle effect”. This is the main reason for the low columbic efficiency and rapid capacity fading.^[2] Moreover, LiPSs shuttling can also result in fast corrosion of the Li anode to lead to an increased cell impedance, which further

1. Introduction

Standing at the gateway to a new era, we have witnessed dramatic changes of energy storage technologies over recent decades, especially the appearance of electric vehicles (EVs) on roads indicates a first step toward a green and smart society. Since the first successful commercialization of the lithium ion (Li-ion) battery by SONY, Li-ion batteries have dominated the energy storage

S. Deng, C. (John) Zhang
College of Materials Science & Engineering
Sichuan University
Chengdu 610065, China
E-mail: chuanfang.zhang@scu.edu.cn

S. Deng, T. Guo, J. Heier, C. (John) Zhang
Laboratory for Functional Polymers
Empa
Swiss Federal Laboratories for Materials Science and Technology
Überlandstrasse 129, Dübendorf CH-8600, Switzerland
E-mail: jakob.heier@empa.ch
S. Deng
Institute of Materials Science and Engineering
Ecole Polytechnique Fédérale de Lausanne (EPFL)
Station 12, Lausanne CH-1015, Switzerland
T. Guo
Key Laboratory of Multifunctional Materials and Structures
Ministry of Education
School of Electronic Science and Engineering
Xi'an Jiaotong University
Xi'an, Shaanxi 710049, China

 The ORCID identification number(s) for the author(s) of this article can be found under <https://doi.org/10.1002/advs.202204930>

© 2022 The Authors. Advanced Science published by Wiley-VCH GmbH. This is an open access article under the terms of the Creative Commons Attribution License, which permits use, distribution and reproduction in any medium, provided the original work is properly cited.

DOI: 10.1002/advs.202204930

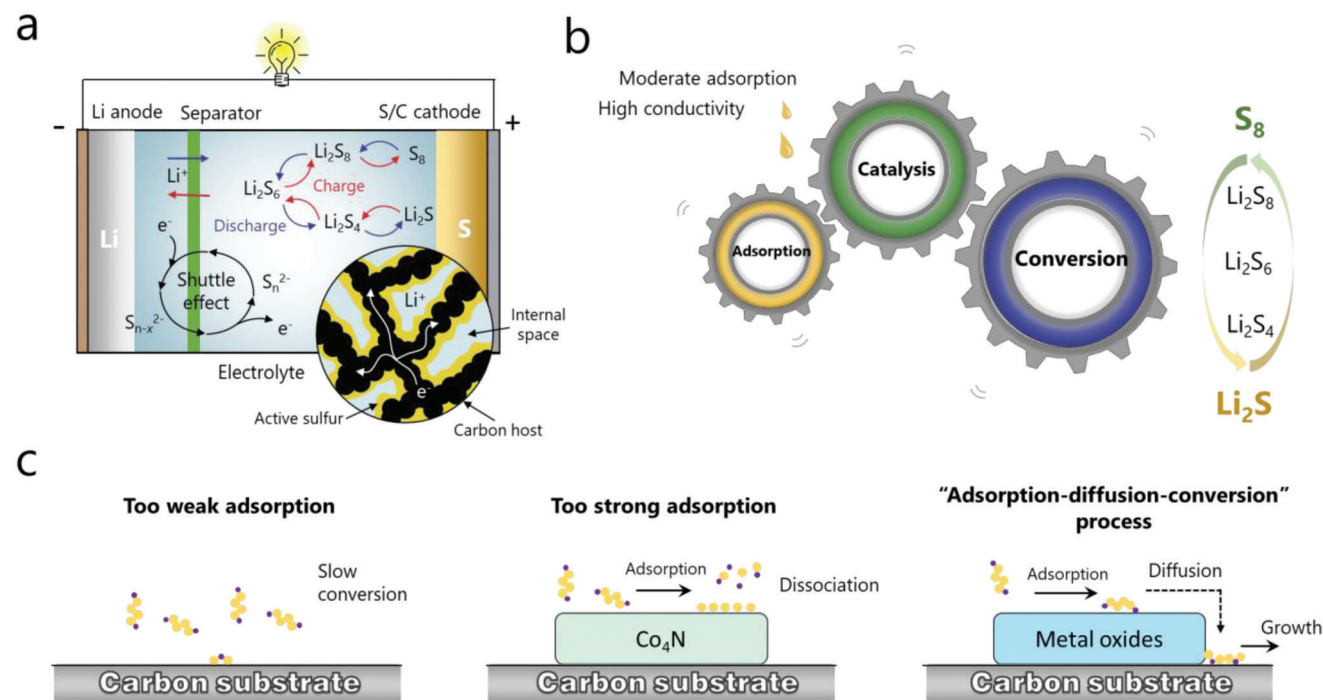


Figure 1. a) Illustration of charge transportation and reversible reaction in Li-S battery. b) The function and basic mechanism of adsorption, catalysis, and conversion. c) Polysulfide behaviors of carbon substrate, Co_4N catalyst, and metal oxide catalyst, respectively.

hampers the batteries' development.^[3] The reaction mechanism is well illustrated in Figure 1a.

Confining active sulfur into porous conductive carbonaceous material was the main approach in the early stages of development.^[1c,2b,4] In this strategy, the LiPSs' escape and shuttling is suppressed by physical spatial confinement, and the sulfur expansion is also accommodated by internal space, which can result in a significant improvement in cycling stability. Examples of carbonaceous hosts include mesoporous carbon, carbon nanotubes (CNTs), carbon nanocages, hierarchical porous carbon, and so on.^[5] These carbonaceous materials, which act as sulfur host, require high conductivity with large surface area and porous structure.^[6] However, a host material with excess porosity and surface area will also lead to negative effects: 1) resulting in a low tapped density cathode which needs large amounts of electrolyte for infiltration; and 2) leading to the formation of excessive cathode electrolyte interface (CEI) and consuming extra electrolyte, since the amount of electrolyte is critical to the pack energy density of batteries.^[7] Therefore, cell parameters such as sulfur loading, tapped density and E/S (electrolyte/sulfur) ratio need to be paid attention to, which is of significance to commercial applications.^[8] In the past few years, we have witnessed Li-S batteries with prominent capacity and superb cyclic performances even at severe environmental conditions enabled by catalytic materials as cathode host or separator interlayer.^[9] The interfacial chemistry—chemical adsorption and catalytic conversion, play the key role to achieving such high cell performances.

Chemical adsorption between adsorption sites and LiPSs can not only anchor polysulfide to alleviate LiPSs mitigation, more importantly, the strong adsorption can also alter the reaction path of LiPSs, thus accelerating the formation of products, resulting

in a catalytic conversion. As catalysis is very important in Li-S chemistry, it can greatly decrease the activation energy with a minor amount of catalyst to improve the sulfur utilization. Meanwhile, it can prevent LiPSs from being accumulated, thus further suppressing the shuttle effect.^[10] Till now, numerous adsorbents have been developed, such as functional groups, heteroatoms, metal compounds, black phosphorus and so forth, with different adsorption strength and mechanism.^[11] Notably, a stronger adsorption does not necessarily correspond to a better catalytic property. Said otherwise, a too strong adsorption can dissociate the original Li-S bond of LiPSs and impedes the LiPSs formation, which could reduce the conversion kinetics. For example, density functional theory (DFT) calculations revealed that the interaction of Li_2S_6 on Co_4N is so strong that the Li-S bond will be broken, resulting in a sulfurized surface of Co_4N similar to CoS_2 (Figure 1c).^[12] Therefore, understanding the adsorption mechanism and screening the optimum binding configurations, as well as deciphering the catalytic activity, are of great importance for effective catalyst material design. Today theoretical models provide valuable insights for the smart design of catalysts and can speed up the search for good materials.^[13] Although recent reviews are available in summarizing those adsorbents and catalytic materials, as well as their synergies, little attention was paid to unraveling basic principles and the internal relationships between adsorption and catalytic property.

Metal oxides (MOs) that combine high polarity, chemical stability and low cost emerge as the most promising catalytic materials in Li-S systems, and which are considered to provide moderate adsorption to polysulfide. So far, many MOs like TiO_2 , MnO_2 , Fe_3O_4 , Co_3O_4 , CeO_2 , etc. were found to possess efficient adsorption and catalytic activities in Li-S chemistry.^[2a,14] However, the

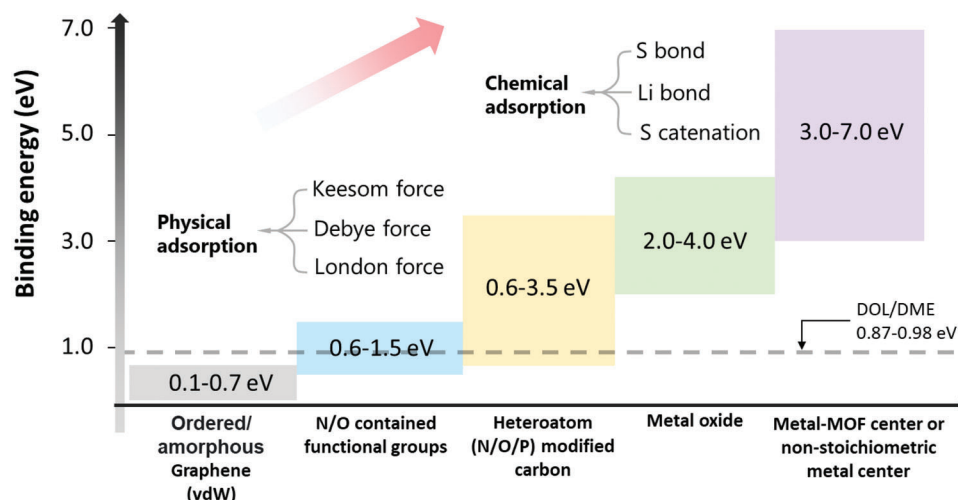


Figure 2. The interactions scope of categorized adsorbents to LiPSs. The binding energies are derived from computations.

inherent poor electrical conductivity nature of MOs is unfavorable for electron transfer and will impede the direct LiPSs conversion on its surface. Thus, an additional diffusion step is generally needed for LiPSs to migrate to the ternary interface between electrolyte, insulating MOs and conductive substrate, resulting in the “adsorption-diffusion-conversion” process (Figure 1c).^[15] Unlike some high conductive catalysts (i.e., metal carbides or nitrides) where adsorption and catalytic conversion can proceed directly on their surface, the extra diffusion step on low conductive MOs requires extra energy, which slows down the reaction kinetics.^[15a] This is a main reason for the limited catalytic effectiveness of low conductive MOs. To overcome this inherent problem, two promising strategies are concluded from the recent literature. One is to introduce oxygen vacancies (OVs). It is reported that oxygen vacancies in metal oxides enhance the intrinsic electron conductivity as well as catalytic activity. OV-rich MOs with altered electron structure manifest conductive properties and can basically change the catalytic process.^[16] The other one is constructing heterostructures. Unlike improving the intrinsic conductivity of MOs, introducing heterostructures can smoothen the “adsorption-diffusion-conversion” process.^[15b] Moreover, the generated heterojunction can show a higher catalytic ability toward LiPSs conversion.^[17] With oxygen vacancies or heterostructures, intriguing performances have been achieved for MOs composite based Li-S batteries.^[18] However, so far, a review that summarizes these two modifications to overcome the insulating properties for achieving high catalytic activity composite materials is still missing.

To fill this gap and figure out the principles, a thorough investigation of MOs electrocatalysts is needed. In this review, we first aim to excavate the underlying mechanism by generalizing different types of interactions between LiPSs and adsorbent and summarize recently developed models and descriptors to evaluate the catalytic activities. Recent works on various MOs’ electrocatalysts in Li-S batteries are subsequently reviewed, in which MOs are employed in either cathode host or separator interlayer. Finally, by combining above catalytic models, MOs with oxygen vacancies and heterostructure engineering are comprehensively elaborated and reviewed with respect to their perspectives. As a

whole, we hope this review offers instructive guidance to explore effective metal oxide-based conductive materials with superior adsorption-catalytic properties for the commercialization of Li-S batteries.

2. Mechanism of Adsorption and Catalysis in Li-S Chemistry

2.1. Adsorption

As we know, the dissolution of intermediate LiPSs into the organic electrolyte causes the “shuttle effect” of LiPSs, leading to capacity fading and low Coulombic efficiency. It should be pointed out that the dissolution is determined by the intermolecular attraction between LiPSs and electrolyte solvent.^[19] Therefore, a stronger attraction from the host is necessary to suppress the dissolution of LiPSs and further realize the suppression of the shuttle effect.

We start the discussion with the interaction between the electrolyte (DOL/DME) and soluble LiPSs (Li_2S_x , $4 \leq x \leq 8$). DFT theory was used to calculate the binding energy value of DOL and DME, which is about 0.87–0.98 eV.^[20] To realize an adsorption effect, the interaction between host and soluble LiPSs should be stronger than this value. When graphene was employed as sulfur host, the binding energy between graphene and LiPSs was calculated as 0.1–0.4 eV, which is smaller than that of the electrolyte.^[21] This is the main reason for massive LiPSs dissolution and the shuttle effect in bare carbon hosts. In order to enhance the adsorption between LiPSs and the conductive host, fabricating polar surface has been proven to be quite effective. As shown in Figure 2, multiple kinds of polar sites have attracted attention like functional groups, heteroatoms (N/O/P etc.), metal based compounds, metal-organic framework (MOF) based composites and so forth, rendering much stronger interactions toward LiPSs.^[22] According to bond strength, these interactions can be divided into physical adsorption and chemical adsorption. The physical adsorption, which is caused by van der Waals (vdW) forces, combines Keesom orientation forces (F_o), Debye induction forces (F_i) and London dispersion forces (F_D),

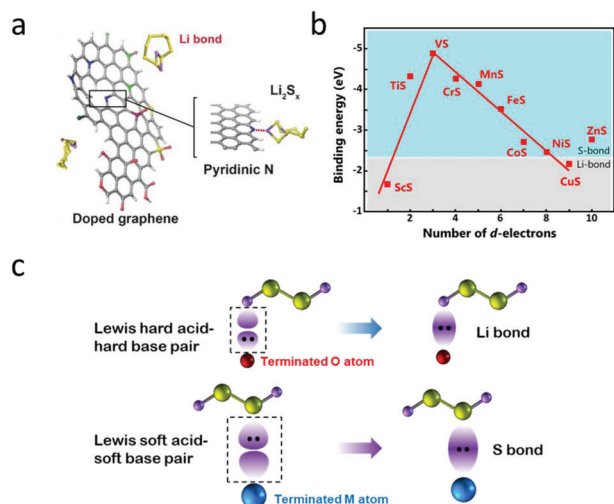


Figure 3. a) Schematic diagram of Li bond in pyridinic N. Reproduced with permission.^[24b] Copyright 2017, Wiley VCH. b) Periodic law of binding energy among first-row TMS. Reproduced with permission.^[28] Copyright 2017, American Chemical Society. c) Schematic diagram of the formation of Li bond and S bond via Lewis acid-base pairs using Li₂S₂ as example.

representing interactions between polar-polar, polar-nonpolar and nonpolar-nonpolar species, respectively.^[23] The interaction between graphene and LiPSs is of this type. However, due to the weak binding characteristic, the physical adsorption is not strong enough to realize stable anchoring of LiPSs. For a strong binding, chemical adsorption is required, which is also the key in the following adsorption study. According to different function principles, we classify these chemical adsorptions into the following categories: Li bond, S bond and sulfur-chain catenation. In this part, the Li bond and S bond will be first introduced below.

2.1.1. Li Bond

The Li bond is formed between the electronegative polar site and terminal Li atom in LiPSs, which can be presented as Li-X (X represent O, N, P, etc.).^[21b,24] A typical example is the Li-pyridinic N (pN) interaction in N-doped graphene (NG) (**Figure 3a**). Such interaction is considered as a kind of dipole-dipole interaction.^[24b] It is worth noting that the Li bond must be distinguished from Keesom interactions, as the Li bond showcases a much higher dipole moment and bond strength. Certainly, the Li bond should also be differentiated from traditional ionic bonds for the much higher binding of the ionic bond. Meanwhile, the formation of an ionic bond is always accompanied by charge transfer, while charge transfer in the Li bond is negligible. Therefore, the Li bond can be defined as a unique bond originating from electrostatic attraction with a binding energy between Keesom interaction and ionic bond.^[25]

Lewis acid-base theory was proposed to explain the formation of Li bonds. In a typical Li-pN interaction, the pN with extra lone pair of electrons in the *p*-orbitals can act as Lewis base, while terminal Li in LiPSs with vacant orbital serves as Lewis acid. As a result, a relatively strong binding is obtained by Lewis acid-base coordination. This theory also explains that only pN in NG can form a Li bond with LiPSs. For other two kinds of N (i.e., pyrrolic

N and graphitic N) without lone pair electrons in their valence orbitals, the interaction between them and LiPSs are simply identified as normal Keesom interaction. Therefore, it is concluded that the fundamental difference between the Li bond and Keesom interaction lies in the availability of lone pair electrons.^[24b,26] In addition, based on HSAB (Hard-Soft-Acid-Base) theory, terminated Li atoms with high positive charge and small size can be considered as hard acid. Thus, Li atoms easily form bonds with a hard base possessing a similar large negative charge and small size atom, which are typically polarized X (O, N, P, etc.) atoms.^[27] This theory provides a new perspective to explain the formation tendency of Li bonds.

2.1.2. S Bond

Except terminal Li that act as hard Lewis acid in Li-bonding, the polysulfide anions (S_x²⁻) can also render it as a soft Lewis base for the lone electron pairs of sulfur. Therefore, in principle, host materials exhibiting soft Lewis acid character can also strongly interact with LiPSs to show Lewis acid-base interaction, such bond is generally called S bond. Different from the Li bond that is mainly based on a Coulombic effect, the S bond has a more covalent nature.^[27,28] In this regard, transition metal (TM) composites possessing vacant *d* orbitals are capable to serve as soft Lewis acid to coordinate with S_x²⁻ to form TM-S bonds. To investigate the effect of *d*-orbital filling on the interaction, theoretical calculations for various TM-S configurations among first-row transition metal sulfides were conducted. An analogous periodic law for S bond was subsequently proposed. As shown in **Figure 3b**, from ScS to ZnS, there are two nearly linear scaling lines where VS lies on the top indicating the strongest binding. Such a volcano-type correlation is the result of the counterbalance between valence electron number and unoccupied *d*-orbital number. This periodic law provides valuable guidance for screening TM and targeting strong adsorption to restrain the shuttle effect.^[28]

For transition metal oxides (TMOs), it can be considered that Li bond and S bond coexist. In most cases, the Li bond dominates the binding energy as most TMOs are oxygen terminated. But in the case of sub-stoichiometric oxides or unsaturated metal, the S bond also contributes significantly to the interaction.^[21b,28] Material that is able to form a Li bond or S bond with LiPSs correspondingly exhibit lithophilic or sulfiphilic behavior, respectively.

To note here, instead of previous classified polar-polar interaction and Lewis acid-base interaction,^[21b,29] we describe chemical adsorption between host and LiPSs as Li bond and S bond, which is more precise to understand the diverse adsorption behaviors. These two bonds are considered as Lewis acid-base interaction. As shown in **Figure 3c**, both bonds originate from the coordination between filled orbitals and vacant orbitals, which are served as Lewis base and Lewis acid, respectively. The HSAB theory can better explain the diverse behaviors of LiPSs, where terminal Li atom and S_x cluster in polysulfide (Li-S_x-Li, 2 < *x* < 8) can be considered as hard acid and soft base, providing vacant orbital and lone electron pairs, respectively. In addition, as the adsorption is specified into orbital hybridization between adsorbents and LiPSs, we can correlate the bond properties to the electron's

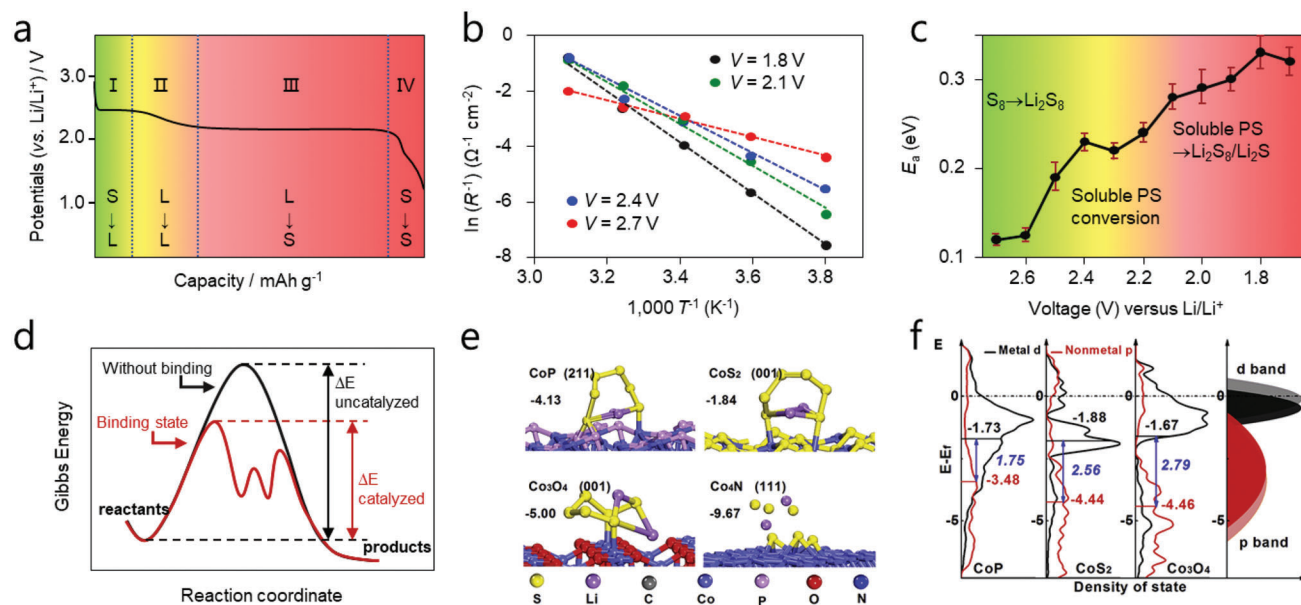


Figure 4. a) Voltage profile of discharge process of Li-S cell. b) Arrhenius plots of the line relationship of charge transfer resistance and temperatures from 1.8–2.1 V. c) Activation energy profiles at different voltages. Reproduced with permission.^[40] Copyright 2021, Wiley VCH. d) Alteration of reaction pathway for binding configuration. e) Binding energies and adsorption configurations of CoP, CoS₂, Co₃O₄, and Co₄N to Li₂S₆. f) DOS analysis of d and p band for CoP, CoS₂, and Co₃O₄, respectively. Reproduced with permission.^[12] Copyright 2018, Elsevier.

occupancy and antibonding state in hybridization orbitals, which provides a new method in catalytic research.^[30]

2.2. Catalysis

In addition to trapping polysulfide via binding to prevent dissolution and shuttling, the reaction kinetics also plays a significant role. Sluggish kinetics always leads to the accumulation of numerous LiPSs at the cathode and inevitably result in LiPSs diffusion. Moreover, arbitrary precipitation is also possible due to the sluggish kinetics, resulting in the formation of large Li₂S particles that are difficult to be reused. Therefore, materials with high catalytic capability can effectively enhance the reaction kinetics which can contribute to suppressing the shuttle effect and ensure uniform precipitation, leading to a high sulfur utilization. In addition, it can also reduce the overpotential and improve the high rate performance. In this part, the basic principles and underlying mechanisms for catalysis are discussed and presented for lithium sulfur chemistry, which is vital for screening high-activity catalysts.

2.2.1. Rate-Determining Step of Li-S Chemistry in Discharge Process

Sulfur reduction during discharging undergoes a complex multistep electrochemical conversion reaction, which can be divided into four steps marked with four regions in **Figure 4a**. Step I is a solid-liquid transition in which the initial S₈ reacts with Li⁺ to form Li₂S₈. Step II is a liquid-liquid transition in which dissolved Li₂S₈ reduces to Li₂S₆ and finally to Li₂S₄. Step III is a liquid-solid transition for the dissolved Li₂S₄ to insoluble Li₂S₂ or Li₂S. Noting that Li₂S₂ and Li₂S coexist, step IV is a solid-solid transition in which the insoluble Li₂S₂ further transfers to insoluble

Li₂S. In particular, due to the non-conductive nature of both Li₂S₂ and Li₂S, the final step suffers from very high polarization,^[31] making the region IV negligible in most cases. Therefore, the whole process during discharging can be considered as the three processes solid-liquid dissolution, liquid-liquid transformation, and liquid-solid precipitation.

To figure out the rate-determining step, the activation energies (E_a) for each step were determined experimentally based on the Arrhenius equation. As shown in **Figure 4c**, the charge transfer resistance (R_{ct}) at each voltage at various temperatures (**Figure 4b,c**) was investigated via impedance techniques.^[32] It was found that the rate-determining step is the final precipitation process, which controls the kinetics of reaction and is responsible for the shuttle effect. Thus, focus should be paid on the precipitation steps when considering the electrocatalytic reaction in Li-S chemistry.

2.2.2. Principles of Li-S Catalysis and D-Band Theory

In Li-S batteries, catalysis which enables fast conversion kinetics by lowering the energy barriers through active sites can be evidenced by some experimental results related to specific electrochemical parameters such as charge transfer impedance, overpotential, Tafel plot, and so on.^[33] However, the intrinsic catalytic activity on each active site and their functions are difficult to be identified and understood, as the catalytic activity is not directly correlated with the above experimental parameters, where the sites numbers or host structures also heavily influence these experimental results. The mechanism of the catalysis still remains unclear. Therefore, understanding the root of catalytic effect in Li-S batteries is of great significance. In addition, besides previous screening of different catalysts which relied on complex trial-

and-error experiments, plenty of high-throughput calculations, and machine learning have been implemented to unfold the mysteries of LiPSs catalytic conversion. In this strategy, simple and easily obtainable physical/chemical properties termed reactivity descriptors were proposed to correlate with reaction energies or activation barriers. Thus, a scaling relationship between descriptors and catalytic activity is established, which is meaningful for the exploration of fundamental catalytic mechanisms and screening high catalytic electrocatalysts.^[34]

As is well documented, the catalytic process of Li-S chemistry is a heterogeneous catalysis. Different from many gas-phase catalytic processes that follow the Eley-Rideal pathway, the Langmuir-Hinshelwood mechanism applies more to the Li-S catalysis with a solid phase product. Thus, the catalytic process toward LiPSs consists of the following steps: the adsorption of LiPSs, diffusion and reaction at the active sites and finally desorption of the product from the catalyst surface. These steps involve the exchange of Li ions and electrons, with the bond breaking and formation between reactant and catalytic active sites.^[34b,35] From this point of view, binding energy which can well describe the bond strength is considered as a descriptor in Li-S catalysis. In a typical adsorption-catalytic process, a strong binding between active site and LiPSs will weaken the S-S bond in the sulfur chain, which makes high order LiPSs easier to be dissociated and converted into low order sulfur chains, effectively promoting LiPSs reduction (Figure 4d). However, too strong interaction with the stable configuration may also impede the transformation and block the surface reaction sites. This phenomenon has been elucidated as “Sabatier principle”, where binding energies and catalytic activities are plotted as a “volcano-type” function.^[36] Thus, Sabatier principle could be a qualitative way to predict the activity of catalysts. To further understand the complex processes, a molecular-level study is needed to be established.

The *d*-band theory proposed by Hammer and Norskov aids the understanding of the bond formation and catalytic activity.^[37] In the *d*-band theory, the *d* band of TMs plays a major role in the interaction with LiPSs, and the band of *d*-state can be approximately considered as a single energy state called *d* band center (ϵ_d). Thus, a stronger adsorption to the LiPSs can be correlated to the up shifting of *d*-band center toward Fermi level, for the up shifting of *d*-band would make antibonding states arising and probably be emptied, thus resulting in an enhanced interaction.^[38] Therefore, the *d*-band center can be considered as a descriptor, where ϵ_d shifts toward the Fermi level corresponding to a strong interaction. When using the *d*-band center as descriptor, different modulations like doping, alloying, strain, etc. that can alter the catalytic properties can be well explained. For example, when alloying metallic Ni with Fe, the coordination number of Ni would be reduced, resulting in the upshift of the *d*-band center toward Fermi level. As a consequence, it brings an enhanced kinetics with a high electrocatalytic activity.^[39] The *d*-band center has also been validated to be an efficient descriptor for many catalytic processes with transition metal catalysts.^[34b]

2.2.3. D-p Model for TM Compound

In *d*-band theory, the metal centers are usually regarded as active sites for the redox reactions and the position of *d*-band

center toward Fermi level is responsible for the catalytic activity. However, this descriptor is not always correct especially in TM compounds. For example, Qian et al. investigated the catalytic properties of various Co based compounds (CoP, CoS₂, Co₃O₄, and Co₄N).^[12] As shown in Figure 4e,f, compared with CoP and CoS₂, Co₃O₄ exhibits both a stronger binding energy and smaller gap between *d*-band center and Fermi level. However, experimental studies showed that CoP possesses the most superior performances as well as the highest catalytic activity rather than Co₃O₄. To explain this, the authors proposed the *p*-band center of anions, *p* orbitals of catalysts, and ascribed the higher catalytic activity of CoP to the narrower gap between *p*-band center of anions and *d*-band center of metals. As shown in Figure 4f, compared with CoS₂ and Co₃O₄, the *p*-band center of CoP shifts closer toward the Fermi level, thus resulting in a narrower energy gap between 3*d* and 2*p* band center. The softer and less electron pulling character of the P atom would increase the energy of bonding state and reduce the energy gap between bonding and anti-bonding orbitals, thus presenting a higher degree of hybridization and contribution to valance electron energy, facilitating the electron exchange and redox dynamics. Meanwhile, a similar work to compare the catalytic activity of Fe based oxide and phosphide compounds was performed by Zhu's group.^[41] They obtained the same conclusion as Qian's work that the higher the shift of the *p*-band center in FeP, the higher the contribution to catalytic activity. Other analogous works also support that a smaller energy band gap between the *d* and *p* bands in TM compounds corresponds to a better catalytic activity, which are all well in agreement with the experimental values.^[42] From these cases, $\Delta\epsilon$ (*p*-*d*) can predict the catalytic activities and can thus also be a good descriptor in TM compounds. Based on this, the *d*-*p* model was subsequently proposed, which provides valuable guidance for rationally screening TM based compound catalysts.

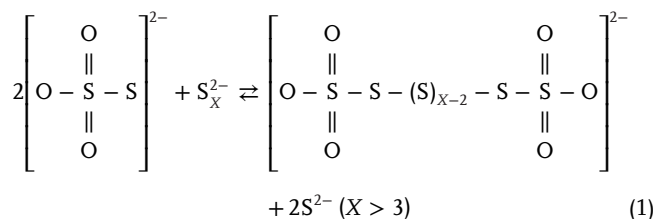
Although the importance of the catalytic effect is gradually being appreciated in Li-S research, the catalysis in Li-S chemistry cannot be considered as a traditional heterogeneous catalysis with gas-phase reactants and product. It should be noted that desorption of solid Li₂S₂/Li₂S is difficult, which would poison the active sites and lead to progressive catalyst deactivation. There are some works that have provided solutions to address the accumulation of S/Li₂S₂/Li₂S. For example, an electrolyte strategy was proposed to realize a full dissolution of Li₂S_x ($1 \leq x \leq 8$) and transfer the solid related reactions into liquid-liquid reactions.^[43] Inspired by this, the concept of “surface cleaning electrolyte additives” was also proposed to sweep and refresh the catalyst surface by dissolving the solid deposits.^[44] These strategies are intended to dissolve Li₂S into electrolyte to maintain the activities of electrocatalysts. In addition, except heterogeneous electrocatalysis, the homogeneous electrocatalysis was also introduced to improve the reaction kinetics in Li-S batteries. These homogeneous electrocatalysts are a kind of soluble small-molecules additives, which are usually called redox mediators (RMs).^[15a,45] In this respect, the RMs enables the full exposure to LiPSs and serve as accelerator to promote the reaction conversion by generating additional pathways. And the coverage of active sites and the degraded activities can be avoided by this strategy. Nevertheless, highly effective catalysts in heterogeneous catalysis are still effective in promoting electrochemical performances by enhancing conversion between

soluble polysulfides and facilitating the precipitation and dissolution of solid $\text{Li}_2\text{S}_2/\text{Li}_2\text{S}$.^[46]

2.3. Thiosulfate/Polysulfide pathway

2.3.1. Sulfur-Chain Catenation

Except for the abovementioned Li bond and S bond mechanism that relied on the surface affinity between host material and LiPSs, another and different chemical approach can also entrap LiPSs by reversibly catenating and grafting polysulfide chains into a kind of sulfur contained complex, a process called sulfur catenation. For example, as a member of promising all solid state battery materials, lithium thiophosphate (Li_3PS_4) can reversibly react with sulfur to yield a family of sulfur-rich lithium polysulfidophosphates (LiPS_{4+n}) with equally high ionic conductivity.^[47] In this process, sulfur atoms were reversibly grafted into PS_4^{3-} through breaking and formation of S–S bonds. Based on this mechanism, Nazar et al. found a kind of thiosulfate groups ($\text{S}_2\text{O}_3^{2-}$) that can also reversibly catenate polysulfide to form a polythionate complex ($\text{O}_3\text{S}-\text{S}_x-\text{S}$).^[48] Specifically, during the discharge process in the Li–S cell, the host such as manganese dioxide can serve as prototype reacting with the initially formed LiPSs to generate the initial thiosulfates. The formed thiosulfate species thereby anchor LiPSs by catenating them through the S–S bond to form surface-bonded intermediates polythionate complexes, and finally convert them into Li_2S via disproportionation (Equation (1)). This new trap mechanism on the surface of MnO_2 with thiosulfate–polythionate conversion has its basics in the so-called “Wackenroder reaction” reported over a century ago.^[49] Apart from MnO_2 , graphene oxide (GO) and MXene was also proposed to function in the same manner.^[48,50] This catenation mechanism is widely existent in Li–S chemistry.^[9a,51]



2.3.2. Polysulfide Mediator

As LiPSs can be reversibly catenated and grafted into a kind of thiosulfate/polythionate species through a sulfur-chain catenation mechanism, it is worth noting that the formed thiosulfate/polythionate can act as polysulfide mediator (endogenous RMs) to further catalyze the conversion of LiPSs.^[48] As shown in Figure 5a, when different hosts (MnO_2 , GO, and Graphene) were immersed in Li_2S_4 solution, it was found that thiosulfate/polythionate active groups are generated on both surfaces of the MnO_2 and GO host, implying that the polysulfide was initially oxidized into a thiosulfate and polythionate complex. Moreover, for the MnO_2/S electrode with a discharge state of 2.15 V, after aging for 20 h (Figures 5b-i and 5-ii), the peaks of thiosulfate have disappeared but the polythionate complex increased. Besides, the

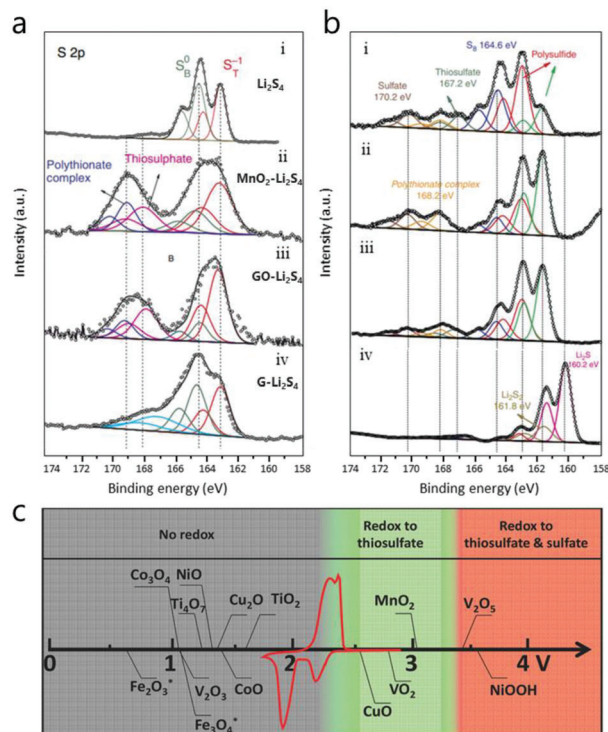


Figure 5. a) The S 2p spectrum of i) Li_2S_4 , ii) $\text{MnO}_2\text{-Li}_2\text{S}_4$, iii) $\text{GO-Li}_2\text{S}_4$ and iv) graphene- Li_2S_4 . Reproduced with permission.^[14] Copyright 2017, Wiley-VCH. b) The S 2p spectrum of S/MnO_2 nanosheet electrodes i) discharged to 2.15 V, ii) discharged to 2.15 V and aged 20 h, iii) discharged to 800 mAh g^{-1} and iv) discharged to 800 mAh g^{-1} and aged for 20 h. All cells were charged at 0.05 C. Reproduced with permission.^[53] Copyright 2021, Wiley-VCH. c) Chemical reactive window for different metal oxides versus Li/Li^+ . Reproduced with permission.^[51a] Copyright 2016, Wiley-VCH.

long-chain LiPSs was transformed to shorter-chain LiPSs, as evidenced by the change in the ratio of terminated S (green, S_T^{-1}) and bridging S (red, S_B^0) peaks. Thus, we conclude that the thiosulfate is able to react with longer-chain LiPSs species to yield shorter LiPSs and polythionate. This process can be considered as a new method to alter the regular reaction pathway of LiPSs.^[51b,52]

However, it should be noted that not all MOs can trigger the initial formation of thiosulfate or catalyze LiPSs conversion in the same manner.^[51a] As shown in Figure 5c, different MOs are distinguished by their chemical reaction window versus Li/Li^+ . The reversible thiosulfate formation can only be triggered in the redox potential window between 2.4–3.05 V such as with VO_2 and MnO_2 . The reversible formation is evidenced in Figure 5b-iii,iv, where both thiosulfate and polythionate were consumed at the end of discharging, while the MOs with values below that window such as TiO_2 and Fe_2O_3 cannot trigger the reaction. In this case, there is only Li bond or S bond formation but thiosulfate/polythionate transformation would not participate in the Li–S reaction. Other MOs such as V_2O_5 with values lying above the window would give rise to over-oxidation of inactive sulfate groups which would result in inferior performances. For these materials lying above the window, an adjusted cycle voltage was recommended to avoid the formation of inactive sulfate species aiming to realize a long cycle life. In short, this so called

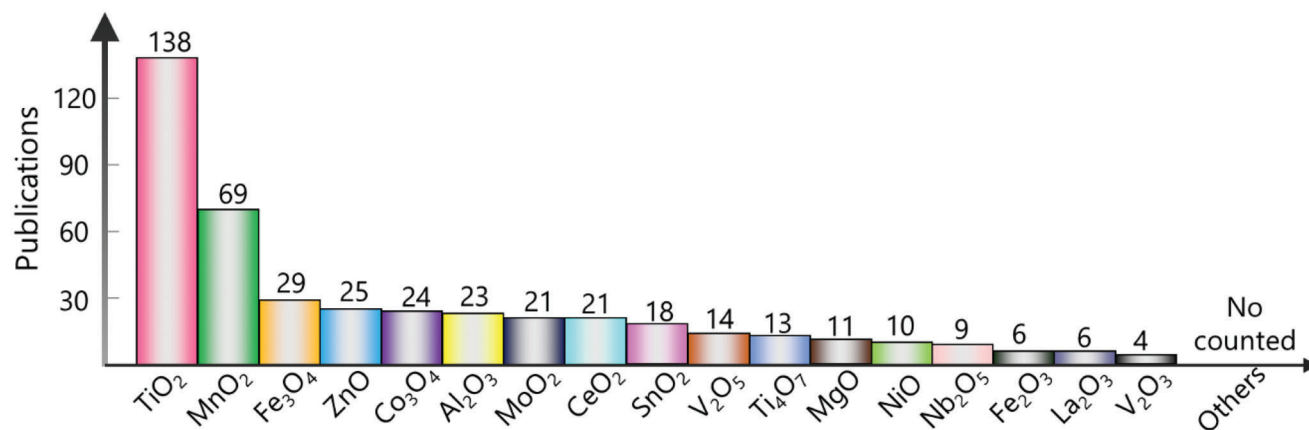


Figure 6. The numbers of publications related to Li-S adsorption or catalysis for various metal oxides.

“Goldilocks” principle provides valuable insights into the correlation of fundamental surface mechanism and cell stability in a thiosulfate/polysulfide pathway, which is essential to design rational MOs for high performance Li-S batteries.

3. Metal Oxides (MOs) Based Conductive Materials

The semiconducting metal oxides (MOs) always exhibit strong polar surfaces derived from high electronegative oxygen terminated surfaces. The exposed anionic surface O²⁻ will have Lewis base character and be thought of possessing lone pair electrons which are responsible for forming a Li bond with LiPSs, giving it potential for providing moderate adsorption and efficient catalytic conversion in Li-S chemistry.^[54] Compared with other metal compounds like metal carbides, sulfides, nitrides and phosphides, MOs can provide a much more stable catalytic surface at a lower cost. However, due to their insulating nature, MOs are not preferable for acting as sulfur hosts. But they could serve as effective additives integrating with carbonaceous materials to fabricate composite hosts by combining both polar adsorption of MOs and conductivity of carbonaceous materials with both electron pathways and ion diffusion channels. For example, Al₂O₃,^[55] SiO₂,^[56] Mg_{0.6}Ni_{0.4}O^[57] and TiO₂^[58] nanoparticles were incorporated in a conductive carbon matrix through mechanical mixing, which delivered improved capacities and cycling stabilities as well as Coulombic efficiencies compared to a bare carbon host or MOs host. Besides mechanical milling, hydrothermal or heat treatment of precursors is a more common strategy to synthesize composites with better integration of MOs and carbon.^[59] In addition, the high adsorption and catalytic effect of MOs was reported to potentially overcome the reliance on LiNO₃ additives, which contributes to a safer Li-S battery. For example, Ding et al. used a RuO₂ catalyst in the sulfur cathode, equipped it with the LiNO₃-free cells and achieved higher capacity and improved capacity retention as compared to their LiNO₃-based counterpart.^[60] **Figure 6** showcases the publication numbers of MOs studied in Li-S batteries in the last decade, showing that TiO₂ and MnO₂ are the most widely studied MOs. **Table 1** summarizes the reported works for MOs based conductive materials employed as cathode and separator interlayer. We note that

MOs as cathode host and interlayer are intrinsically the same, in which MOs are equivalently responsible for accelerating transfer conversion and Li₂S precipitation. In the following section, some typical MOs (i.e., TiO₂, Ti₄O₇, MnO₂, Fe₃O₄, Co₃O₄, MoO₂, CeO₂, and SnO₂) will be briefly discussed.

3.1. Titanium Oxides

TiO₂ is the natural oxide of titanium with four types of crystallographic forms including anatase (α -TiO₂), rutile (β -TiO₂), brookite (γ -TiO₂) and bronze (B-TiO₂), where the bronze is the least stable.^[117] DFT calculations have shown that the binding energies between α - and β -TiO₂ to LiS[•] (represent LiPSs) is 2.30 and 2.18 eV, respectively (**Figure 7a,b**).^[118] In the α -TiO₂/Li₂S₄ composite, the S-Ti-O signal and Raman peak shifts suggest bond formation between α -TiO₂ and Li₂S₄ (**Figure 7c**). However, the signal could not be detected in either the β - or γ -TiO₂/Li₂S₄ composite (**Figure 7d,e**), implying weaker bindings with Li₂S₄ than α -TiO₂.^[58] Similarly, the adsorption behavior of B-TiO₂ was also evaluated by DFT calculation, showing a weaker binding with Li₂S₈ (1.63 eV) than that of α -TiO₂ (1.83 eV). However, when CNT@B-TiO₂ and CNTs@ α -TiO₂ were designed as separator interlayer, respectively, CNTs@B-TiO₂ delivered a superior performance with higher capacity and more stable cycling than CNTs@ α -TiO₂. Such result was attributed to the diverse diffusion properties. DFT analysis demonstrated a smaller Li⁺ diffusion barrier of B-TiO₂ (0.58 eV) than α -TiO₂ (0.71 eV), highlighting the importance of diffusion properties of MOs in the typical adsorption-diffusion-conversion process.^[119]

Despite effective entrapment of LiPSs, the low conductivity of TiO₂ renders quite undesirable electrochemical performance. In contrast, titanium based oxide Ti₄O₇ possesses high conductivity even showing metallic properties (**Figure 7f**).^[120] When Ti₄O₇ is directly employed as sulfur host, the Ti₄O₇/S provides a reversible discharge capacity of 1070 mAh g⁻¹ at 0.2 C, and reversible cyclic stability of over 500 cycles.^[121] Besides conductivity, Ti₄O₇ also exhibits a rare sulfiphilic surface different from most MOs with a lithophilic surface, which enables Ti₄O₇ to form S bonds with LiPSs rather than Li bonds. To understand the surface properties, comparison is made between TiO₂ (rutile

Table 1. Examples of performances of different MO_x based conductive materials.

MO _x based conductive materials	Application	Cathode area loading (sulfur content)/separator thickness	Electrolyte/sulfur (E/S) ratio	Capacity retention (rate, cycles)	Capacity decay per cycle	Ref.
G/TiO ₂	Cathode	1.5–2 mg cm ⁻² (60%)	NA	737 mAh g ⁻¹ (0.5 C, 100 cycles)	0.25%	[61]
CP@TiO ₂	Cathode	2 mg cm ⁻² (40%)	NA	850 mAh g ⁻¹ (0.5 C 200 cycles)	0.24%	[62]
G/TiO ₂	Separator	0.51 mg cm ⁻² (51.2%)/3 μm	NA	1040 mAh g ⁻¹ (0.5 C, 300 cycles)	0.00003%	[63]
HCNF@TiO ₂	Cathode	2 mg cm ⁻² (70%)	NA	380 mAh g ⁻¹ (1 C, 500 cycles)	0.12%	[64]
TiO ₂ /G/NPCDs	Cathode	1.2 mg cm ⁻² (55%)	NA	618 mAh g ⁻¹ (1C, 500 cycles)	0.074%	[59a]
MH-SiO ₂ @TiO ₂	Cathode	NA (80%)	13 μL mg ⁻¹	264 mAh g ⁻¹ (1 C, 1000 cycles)	0.066%	[65]
CNT-T2@TiO ₂	Separator	1.7 mg cm ⁻² (60%)/6 μm	NA	803 mAh g ⁻¹ (0.1 C, 200 cycles)	0.25%	[66]
C@TiO ₂ @C	Cathode	2.5 mg cm ⁻² (76.4%)	NA	511 mAh g ⁻¹ (2 C, 500 cycles)	0.068%	[67]
SDC@TiO ₂	Cathode	2 mg cm ⁻² (60%)	NA	569 mAh g ⁻¹ (1.5 A g ⁻¹ , 1500 cycles)	0.024%	[68]
MWCNTs@TiO ₂ QDs	Separator	0.8 mg cm ⁻² (60%)/5 μm	NA	610 mAh g ⁻¹ (0.5 C, 600 cycles)	0.073%	[69]
C-Co/TiO ₂	Cathode	1.5 mg cm ⁻² (70%)	NA	466 mAh g ⁻¹ (1 C, 300 cycles)	0.15%	[70]
CNT@TiO _{2-x}	Cathode	2.2 mg cm ⁻² (72.9%)	12 μL mg ⁻¹	590 mAh g ⁻¹ (1 C, 500 cycles)	0.053%	[16]
TiO ₂ -MXene	Separator	1.2 mg cm ⁻² (70%)/5 μm	NA	576 mAh g ⁻¹ (2 C, 1000 cycles)	0.028%	[71]
TiO-TiO ₂ /PPy	Cathode	1 mg cm ⁻² (75%)	30 μL mg ⁻¹	412 mAh g ⁻¹ (1 C, 1000 cycles)	0.041%	[72]
TiC@C-TiO ₂	Cathode	2.3 mg cm ⁻² (74.2%)	10 μL mg ⁻¹	603 mAh g ⁻¹ (0.5 C, 160 cycles)	0.148%	[73]
ANDC/TiO _{2-x}	Cathode	1.8 mg cm ⁻² (75%)	NA	995 mAh g ⁻¹ (0.5 C, 500 cycles)	0.042%	[74]
TiO ₂ -CNFs@void@TiN@C	Separator	1.5 mg cm ⁻² (68%)/50 μm	20 μL mg ⁻¹	676 mAh g ⁻¹ (1 C, 1000 cycles)	0.054%	[75]
OV-TiO _{2-x} @NC	Cathode	1.6 mg cm ⁻² (78.3%)	15 μL mg ⁻¹	792 mAh g ⁻¹ (1 C, 2000 cycles)	0.013%	[18b]
CCC@TiO ₂ -TiN	Cathode	3.5 mg cm ⁻² (60%)	NA	821 mAh g ⁻¹ (0.5 C, 500 cycles)	0.071%	[76]
Co ₃ O ₄ -TiO ₂ -HPs	Cathode	1.0 mg cm ⁻² (75%)	NA	416 mAh g ⁻¹ (10 C, 500 cycles)	0.07%	[77]
H-TiO ₂ /r-GO-1	Cathode	1.5 mg cm ⁻² (80%)	15 μL mg ⁻¹	656 mAh g ⁻¹ (1 C, 1000 cycles)	0.023%	[78]
MnO ₂ @HCF	Cathode	3.5 mg cm ⁻² (80%)	NA	662 mAh g ⁻¹ (0.5 C, 300 cycles)	0.088%	[79]
PEDOT/MnO ₂	Cathode	NA (87%)	NA	545 mAh g ⁻¹ (0.5 C, 200 cycles)	0.20%	[80]
MnO ₂ /GO/CNTs	Cathode	2.8 mg cm ⁻² (90%)	NA	963 mAh g ⁻¹ (0.2 C, 100 cycles)	0.239%	[81]
HCNF@δ-MnO ₂	Separator	2.2 mg cm ⁻² (80%)/2 μm	NA	856 mAh g ⁻¹ (0.5 C, 200 cycles)	0.13%	[82]
p-CNT@Void@MnO ₂	Cathode	0.65–1.06 mg cm ⁻² (64.9%)	NA	526 mAh g ⁻¹ (1 C, 100 cycles)	0.13%	[83]
NHCSs@MnO ₂	Cathode	1.9 mg cm ⁻² (69.5%)	10 μL mg ⁻¹	737 mAh g ⁻¹ (0.5 C, 1000 cycles)	0.041%	[84]
G/CNT@MnO ₂	Cathode	1.5–2 mg cm ⁻² (81.8%)	NA	591 mAh g ⁻¹ (1 C, 200 cycles)	0.39%	[85]
MnO ₂ @d-Ti ₃ C ₂	Cathode	3.7 mg cm ⁻² (69.5%)	NA	474 mAh g ⁻¹ (1 C, 500 cycles)	0.052%	[86]
NMRC@MnO ₂	Cathode	1.8 mg cm ⁻² (72%)	NA	590 mAh g ⁻¹ (2 C, 1000 cycles)	0.045%	[87]
PANI-MnO ₂	Cathode	1.5 mg cm ⁻² (66%)	15 μL mg ⁻¹	826 mAh g ⁻¹ (1 C, 500 cycles)	0.055%	[88]
MnO ₂ @rGO	Cathode	4 mg cm ⁻² (70%)	4 μL mg ⁻¹	578 mAh g ⁻¹ (0.2 C, 100 cycles)	0.17%	[89]
3DIS@MnO ₂	Cathode	1.4 mg cm ⁻² (91.5%)	NA	409 mAh g ⁻¹ (10 C, 900 cycles)	0.059%	[90]
YSC@Fe ₃ O ₄	Cathode	5.5 mg cm ⁻² (80%)	NA	854 mAh g ⁻¹ (0.1 C, 200 cycles)	0.11%	[91]
PG-450-Fe ₃ O ₄	Separator	0.6 mg cm ⁻² (60%)/15 μm	NA	732 mAh g ⁻¹ (1 C, 500 cycles)	0.027%	[92]
Fe ₃ O ₄ -NC@ACC	Cathode	4.7 mg cm ⁻² (67%)	NA	780 mAh g ⁻¹ (0.2 C, 1000 cycles)	0.03%	[93]
Fe ₃ O ₄ /CNSs	Separator	1.5 mg cm ⁻² (70%)/8.5 μm	12 μL mg ⁻¹	610 mAh g ⁻¹ (1 C, 1000 cycles)	0.027%	[94]
Fe ₃ O ₄ -PNCT-1	Cathode	1.5 mg cm ⁻² (70%)	NA	612 mAh g ⁻¹ (1 C, 1000 cycles)	0.03%	[95]
3DOMPPy@ZnO	Cathode	NA (60.7%)	NA	795 mAh g ⁻¹ (0.1 C, 300 cycles)	0.06%	[96]
1D ZnO/2D G	Separator	1.1 mg cm ⁻² (70%)/71.2 μm	25 μL mg ⁻¹	765 mAh g ⁻¹ (2 C, 300 cycles)	0.12%	[97]
rGO@ZnO QDs	Cathode	1 mg cm ⁻² (70%)	NA	674 mAh g ⁻¹ (1 C, 400 cycles)	0.067%	[98]
N-Co ₃ O ₄ @N-C/rGO	Cathode	5.89 mg cm ⁻² (75%)	NA	568 mAh g ⁻¹ (0.2 C, 500 cycles)	0.062%	[99]
Co ₃ O ₄ /ACNT	Cathode	1.1 mg cm ⁻² 1.2 (58.73%)	NA	694 mAh g ⁻¹ (0.2 C, 550 cycles)	0.056%	[100]
RCE-Co ₃ O ₄ @G	Cathode	0.8 mg cm ⁻² (71.63%)	NA	727 mAh g ⁻¹ (0.2 C, 350 cycles)	0.026%	[101]
Co ₃ O ₄ /C	Cathode	1.4 mg cm ⁻² (70%)	20 μL mg ⁻¹	520 mAh g ⁻¹ (1 C, 500 cycles)	0.083%	[102]
MoO ₃ /MoO ₂ -CP	Cathode	NA (65.5%)	NA	828 mAh g ⁻¹ (0.5 C, 500 cycles)	0.016%	[103]
MoO ₂ @CNT	Separator	1.7 mg cm ⁻² (75%)/15 μm	NA	540 mAh g ⁻¹ (1 C, 700 cycles)	0.066%	[104]
CeO ₂ /MMNC	Cathode	3.4 mg cm ⁻² (70%)	NA	611 mAh g ⁻¹ (0.5 C, 200 cycles)	0.043%	[6a]
CeO ₂ /CNF	Cathode	8.6 mg cm ⁻² (70.2%)	NA	897 mAh g ⁻¹ (0.1 C, 30 cycles)	0.76%	[105]

(Continued)

Table 1. (Continued).

MO _x based conductive materials	Application	Cathode area loading (sulfur content)/separator thickness	Electrolyte/sulfur (E/S) ratio	Capacity retention (rate, cycles)	Capacity decay per cycle	Ref.
CNTs/SnO ₂ QDs	Cathode	2 mg cm ⁻² (70.3%)	NA	550 mAh g ⁻¹ (0.1 C, 700 cycles)	0.092%	[106]
T-PPy@SnO ₂	Cathode	2 mg cm ⁻² (64.7%)	NA	542 mAh g ⁻¹ (1 C, 500 cycles)	0.05%	[107]
ALD-V ₂ O ₅ @3DNG	Cathode	3.3 mg cm ⁻² (80%)	NA	542 mAh g ⁻¹ (2 C, 350 cycles)	0.053%	[108]
V ₂ O ₅ NWs/GNS	Separator	1.5 mg cm ⁻² (70%)/40 μm	NA	326 mAh g ⁻¹ (2 C, 1000 cycles)	0.061%	[109]
HCS@Ti ₄ O ₇	Cathode	NA (70%)	NA	609 mAh g ⁻¹ (0.5 C, 800 cycles)	0.06%	[110]
CF@CNTs mg ⁻¹ O	Cathode	1.2 mg cm ⁻² (49%)	NA	390 mAh g ⁻¹ (2 C, 800 cycles)	0.06%	[111]
NiO-CNT	Cathode	2.1 mg cm ⁻² (64.8%)	16 μL mg ⁻¹	609 mAh g ⁻¹ (0.1 C, 160 cycles)	0.216%	[112]
MCM/Nb ₂ O ₅	Cathode	1.5 mg cm ⁻² (60%)	NA	650 mAh g ⁻¹ (2 C, 500 cycles)	0.092%	[113]
KB/Fe ₂ O _{3-x}	Cathode	12.73 mg cm ⁻² (70%)	10 μL mg ⁻¹	612 mAh g ⁻¹ (0.05 C, 60 cycles)	0.21%	[114]
10La ₂ O ₃ -NMC	Cathode	NA (60%)	NA	475 mAh g ⁻¹ (5 C, 100 cycles)	0.21%	[115]
G/G-V ₂ O ₃	Cathode	1.4–1.6 mg cm ⁻² (78.3%)	10 μL mg ⁻¹	540 mAh g ⁻¹ (2 C, 1000 cycles)	0.046%	[116]

NA: not available

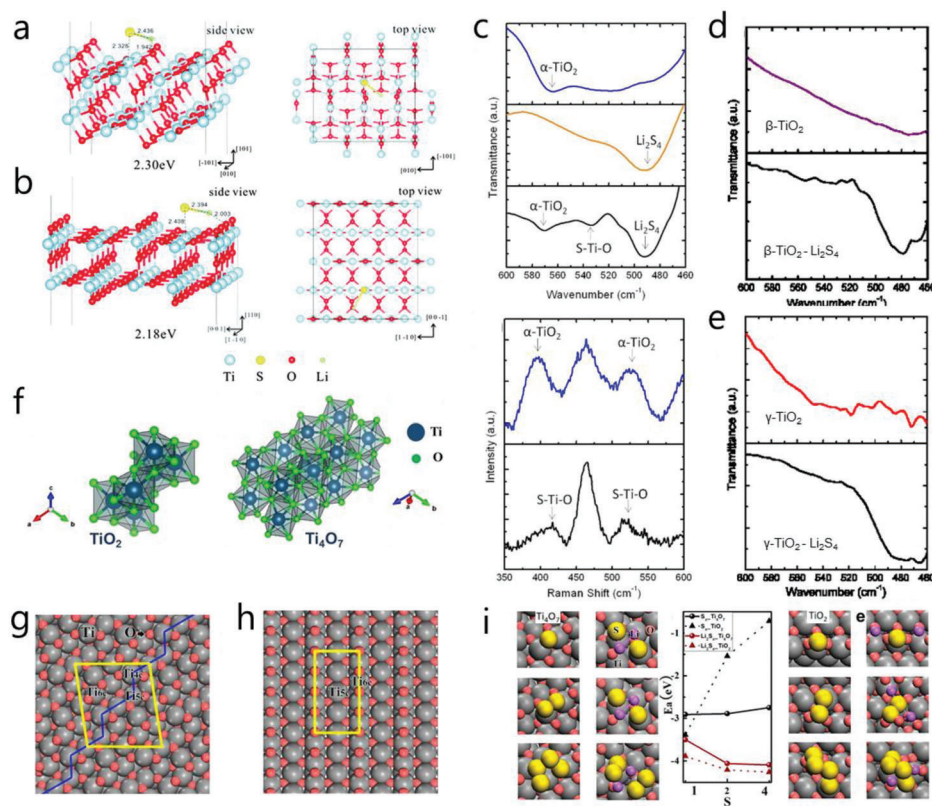


Figure 7. Adsorption configuration of LiS on a) anatase (101) and b) rutile (110) TiO₂. Reproduced with permission.^[118] Copyright 2016, Royal Society of Chemistry. c) FTIR and Raman spectra of α-TiO₂ and α-TiO₂/Li₂S₄ composite. FTIR spectra of d) β-TiO₂ and β-TiO₂/Li₂S₄ and e) γ-TiO₂ and γ-TiO₂/Li₂S₄. Reproduced with permission.^[158] Copyright 2012, American Chemical Society. f) Crystal structure of TiO₂ and Ti₄O₇. Reproduced with permission.^[124] Copyright 2022, Wiley-VCH. Schematics of g) Ti₄O₇ (1–20) and h) TiO₂ (110) surfaces. i) DFT analysis of the adsorption to S species of Ti₄O₇ and TiO₂, respectively. Reproduced with permission.^[122] Copyright 2014, American Chemical Society.

as example) and Ti₄O₇. As shown in Figure 7g, three different Ti atoms of Ti_{4c}, Ti_{5c} and Ti_{6c} represent the coordination number of 4, 5 and 6, respectively, where Ti_{4c} and Ti_{5c} is unsaturated. TiO₂ contains Ti_{5c} and Ti_{6c} in a ratio of 1:1, suggesting the unsaturated Ti fraction is 50%. Whereas in Ti₄O₇ (Figure 7h), the unsaturated Ti ratio is 62.5%, with low-coordinated Ti_{4c} and Ti_{5c} arranged in

the step sites highlighted as a blue line. DFT calculations suggest that the moderate S bond dominates the interaction with LiPSs rather than the Li bond on the Ti₄O₇ surface (Figure 7i).^[122]

The metallic Ti₄O₇ can afford a sulphophilic surface, which is promising as a sulfur host in Li–S batteries. However, the fabrication of Ti₄O₇ was complex, generally requiring harsh conditions

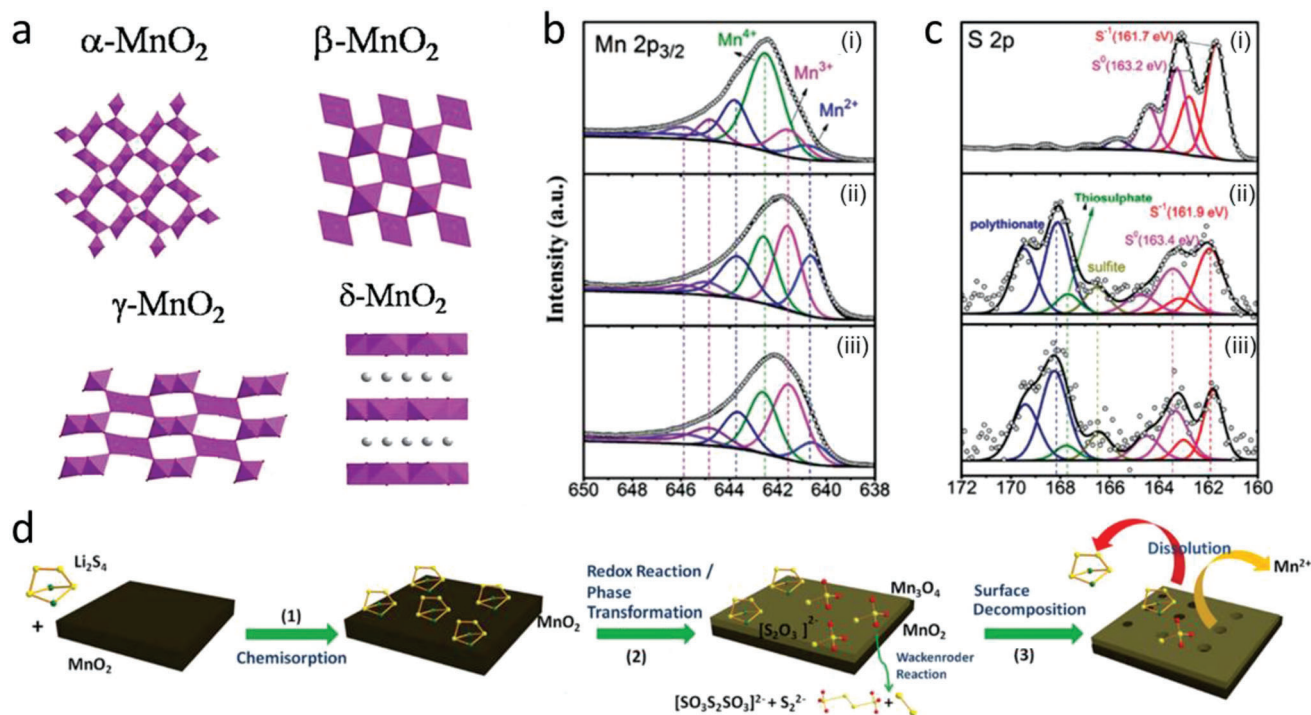


Figure 8. a) The structure of α , β , γ , and δ -MnO₂. Reproduced with permission.^[125] Copyright 2015, Royal Society of Chemistry. b) Mn 2p_{3/2} XPS spectrum of i) γ -MnO₂, ii) γ -MnO₂-Li₂S₄ after 0.5 h, and iii) γ -MnO₂-Li₂S₄ after 5 days. c) S 2p spectrum of i) Li₂S₄, ii) γ -MnO₂-Li₂S₄ after 0.5 h, and iii) γ -MnO₂-Li₂S₄ after 5 days. d) Schematic illustration of the interaction between γ -MnO₂ and Li₂S₄, which concomitant with the surface decomposition of Mn₃O₄. Reproduced with permission.^[126] Copyright 2017, Wiley-VCH.

such as high temperatures of around 1000 °C and a pure reduction atmosphere.^[14] Although relatively cost-effective mild methods were proposed recently,^[123] it is still a challenge to construct a nanostructured and flexible Ti₄O₇ conductive framework.

3.2. Manganese Oxides

MnO₂ is the most common manganese based oxide, which occurs naturally as blackish or brown mineral pyrolusite. Similarly, MnO₂ also has four common polymorphs (α , β , γ , and δ -MnO₂, **Figure 8a**).^[125] It is worth noting that the surface of MnO₂ is always nonstoichiometric with oxygen deficiency.^[14] Benefited with its unique characteristics, MnO₂ is effective in the Li-S catalytic process and was extensively investigated and utilized in Li-S batteries. For example, δ -MnO₂ nanosheets were initially applied as sulfur host to investigate the adsorption to LiPSs.^[48] As detailed before, MnO₂ can act as a prototype to react with initially formed LiPSs to generate the surface-bound intermediate thiosulfate, which serves as a redox mediator to further catenate and react with LiPSs via disproportionation. It was proposed that only metal oxides with a suitable redox potential window can trigger the thiosulfate formation.^[51a] Likewise, this so called “Wackender reaction” in δ -MnO₂ was also found in γ -MnO₂. It was found that the surface phase transformation from MnO₂ to Mn₃O₄ was accompanied by the redox reaction between LiPSs and prototype γ -MnO₂ host.^[126] As shown in **Figure 8b**, compared with pristine MnO₂, after being treated with LiPSs, MnO₂ was partially converted into lower valence species with

significantly increased Mn³⁺ and Mn²⁺ peaks, which is accordant with the generation of Mn₃O₄ detected by XRD. Meanwhile, in the S 2p spectrum (**Figure 8c**), Li₂S₄ was oxidized into thiosulfate/polythionate species. Thus, the initial MnO₂ partially reacts with Li₂S₄ into thiosulfate/polythionate species and Mn₃O₄, which further facilitates LiPSs conversion. Notably, the decreased intensity of Mn²⁺ (**Figure 8b**) suggests the dissolution of Mn²⁺ in DME, which would result in a slight capacity degradation. The whole process for the proposed mechanism is depicted in **Figure 8d**. α or β -MnO₂ have also been investigated in Li-S batteries.^[127] Although numerous works were established for the MnO₂, however, the interactions and catalytic effect between different crystal phases (α , β , γ , and δ) and LiPSs are yet to be resolved.

3.3. Iron and Cobalt Oxides

Iron-based oxides, for example wüstite (FeO), hematite (α -Fe₂O₃), maghemite (γ -Fe₂O₃) and magnetite (Fe₃O₄) with abundant reserves and low costs, possess an excellent polar adsorption and catalytic effect to LiPSs.^[128] Among them, Fe₃O₄, the most widely studied iron oxide, possesses a relatively high electronic conductivity and prominent anchoring ability. Due to the superior advantages of both high polarity and conductivity, Fe₃O₄ based conductive compounds are expected to realize high performance in Li-S batteries. For example, a yolk-shelled carbon@Fe₃O₄ nanobox was designed as sulfur host (**Figure 9a**). With the chemical interaction in the Fe₃O₄ core and physical blocking in the carbon

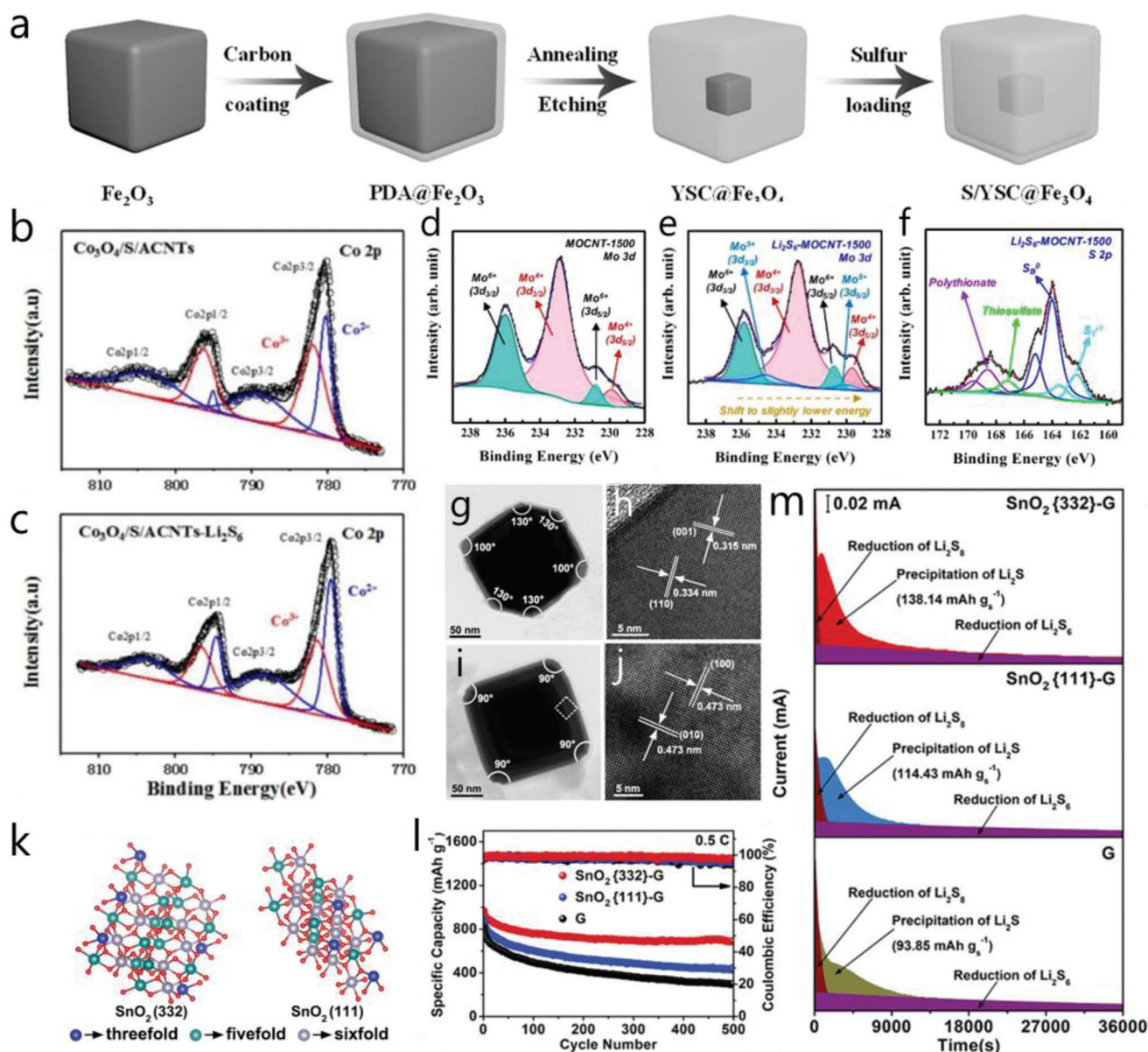


Figure 9. a) Schematic diagram of synthesis of S/YSC@Fe₃O₄ composite. Reproduced with permission.^[91] Copyright 2017, Wiley-VCH. XPS spectra of Co 2p in b) Co₃O₄/S/ACNT and c) Co₃O₄/S/ACNT-Li₂S₆ composites. Reproduced with permission.^[100] Copyright 2019, American Chemical Society. XPS spectra of Mo 3d in d) MOCNT-1500 and e) Li₂S₆-MOCNT-1500 composite. f) XPS spectra of S 2p in Li₂S₆-MOCNT-1500 composite. Reproduced with permission.^[104] Copyright 2020, American Chemical Society. g, i) TEM images of SnO₂ (332) and (111) facets and h, j) the corresponding HRTEM images of the selected region. k) Schematic model of SnO₂ (332) and (111) facets. l) Cyclic performances of SnO₂-G (332) and SnO₂-G (111) cells at 0.5 C. m) Potentiostatic precipitation of SnO₂ (332)-G, SnO₂ (111)-G, and G electrode. Reproduced with permission.^[133] Copyright 2021, Wiley-VCH.

shell, this synergistic effect enabled a high sulfur loading and sulfur content (5.5 mg cm⁻² and 80 wt%), achieving a high area capacity of 6.97 mAh cm⁻² at 0.1 C and decent stability over 200 cycles.^[91] Recently, as metal-organic frameworks (MOFs) have attracted public attention because of their controllable porous structures and porosities, a MOF-derived carbon encapsulated Fe₃O₄ (Fe₃O₄@C) was proposed as sulfur host to mediate polysulfide redox reaction. Benefitting from the strong adsorption of metal oxides and hierarchical porous structures inheriting from MOFs, an excellent performance was achieved.^[129] In addition,

it is proposed to be effective to couple a carbon substrate with ultra-small Fe₃O₄ nanoparticles where Fe₃O₄ NPs act as an efficient LiPSs trapping and active center, promoting the utilization of sulfur materials,^[93,94,128a,129,130] which gained much attention from researchers.

Similar to Fe₃O₄, Co₃O₄ also gained attention due to higher conductivity than most metal oxides and similar non-stoichiometric characteristics with two different valence pair states of metal. Recently, researchers found that the valence pair state of Co²⁺ and Co³⁺ in Co₃O₄ can serve as redox pair that can

affect the redox of LiPSs in Li–S chemistry. Figures 9b and 9c show the XPS spectra of Co 2*p* in Co₃O₄ and Co₃O₄·Li₂S₆, where the peaks of Co₃O₄ can be divided into two valance states of Co²⁺ and Co³⁺. After contacting with Li₂S₆, the intensity of the Co³⁺ peak decreased and Co²⁺ increased, which results in the appearance of thiosulfate and polythionate, thus demonstrating the electron transfer from Li₂S₆ to Co₃O₄.^[100] Such phenomenon is similar to that of MnO₂, where MnO₂ also displays multiple valance states at the surface with a main valance of Mn⁴⁺ and other valances of Mn³⁺ and Mn²⁺.^[126] Due to the superior properties of Co₃O₄, decent performances could be realized. Park et al. designed a multidimensional architecture with N-doped graphene and Co₃O₄ nanoparticles encapsulated CNT branches to combine the strong affinity and enhanced kinetics of Co₃O₄ and confined porous structure, realizing a capacity of 5.62 mAh cm^{−2} at the high loading of 6.5 mg cm^{−2}.^[131]

3.4. Other Metal Oxides

MoO₂ has an oxidized surface where Mo⁶⁺ and Mo⁴⁺ coexist, which give rise to high LiPSs conversion kinetics. Figure 9d,e shows the Mo 3*d* in XPS of MoO₂ and MoO₂·Li₂S₆ based composite, respectively. Compared with MoO₂, after interaction with Li₂S₆, a slight decrease of the Mo⁶⁺ peak and a newly appearing Mo⁵⁺ state were found, which indicates a surface redox reaction between MoO₂ and Li₂S₆. Besides, the XPS in S 2*p* shows the formation of thiosulfate/polythionate in Li₂S₆ after contacting with MoO₂ (Figure 9f), which facilitates the LiPSs adsorption and redox conversion.^[104] Lanthanide oxides stand out as efficient catalysts in electrocatalysis due to the moderate band gap as well as multiple valance states,^[132] where CeO₂ is prominent as LiPSs catalyst. Generally, on CeO₂ surface, except Ce⁴⁺ valance, Ce³⁺ also exist associated with oxygen vacancies.^[132b] The high catalytic ability enables a decent applicable Li–S battery performance. For example, a CeO₂ decorated carbon nanofiber as sulfur host (S@CeO₂@CNF) was designed and achieved a high initial capacity of 8.4 mAh cm^{−2} at a high sulfur loading of 8.6 mg cm^{−2} and retained more than 30 cycles.^[105]

SnO₂ was considered as an efficient catalyst in Li–S chemistry. However, it was reported that the catalytic activity of SnO₂ is greatly influenced by different crystal facets. As shown in Figure 9g–k, the nano-octahedra SnO₂ with two diverse crystal facets of [332] and [111] were typically synthesized and anchored on reduced graphene oxide (G). Compared with SnO₂ [111]-G and G electrode, SnO₂ [332]-G exhibited a more superior cyclic performance (Figure 9l). Moreover, in potentiostatic precipitation tests of Li₂S, as shown in Figure 9m, the higher precipitation capacity of SnO₂ [332]-G reveals a lower nucleation barrier of Li₂S, confirming the improved catalytic property. The improved catalytic activity and cyclic performance is attributed to the more abundant unsaturated-coordinated Sn sites on the [332] plane. As a results, with a higher catalytic activity of [332], the SnO₂ [332]-G cell achieved the area capacity of 6.93 mAh cm^{−2} over 100 cycles with a high sulfur loading of 8.12 mg cm^{−2}.^[133]

Except single metal oxides, the synergism of bimetallic oxides was also explored in terms of LiPSs engineering. A Fe and V coordinated bimetallic oxide FeVO₄ nanocatalyst with 3D ordered structure was used to modify the separator for achieving the

restraining of LiPSs diffusion and boosting the conversion kinetics of sulfur species. It was demonstrated that the FeVO₄ can effectively enhance the anchoring and catalytic activity toward LiPSs compared with single metal oxides of Fe₂O₃ and V₂O₅. In Li–S pouch cells, the FeVO₄/CNT modified separator delivered an initial capacity of 6.5 mAh cm^{−2} at 0.2 C under a high sulfur loading of 6.1 mg cm^{−2}, lean electrolyte with E/S ratio of 5 μL mg^{−1} and N/P ratio of 2, achieving an energy density up to 341 Wh kg^{−1}.^[134]

The above discussion provides examples using various MOs catalysts employed as sulfur host in cathodes or separator interlayers of Li–S batteries. In principle, to achieve a high sulfur loading and energy density performance, it is necessary to decrease the amount of non-active material such as MOs or conductive substrate. Thus, developing effective MOs with high adsorption–catalytic activity is essential and considered to be the main topic of research. However, it is hard to make intuitive comparison and screen the most effective MOs electrocatalyst, because different bulk phases and crystal facets may deliver different activities. And other features like shapeable, durability, or availability also matter.

Nevertheless, it is worth noting that multiple valances on the surface of MOs are favored for realizing significant adsorption and catalytic properties toward LiPSs, where the redox valance pair would enable the formation of thiosulfate/polythionate, thus facilitating the adsorption–catalysis process. This can be recognized as a dual chemical adsorption mode which combines both sulfur-chain catenation and Li/S bond mechanism. A similar example can be found in the comparison between MXene and GO substrates. Both of which can provide –OH groups that can catenate sulfur-chain into the thiosulfate/polythionate mediator. However, after consuming the available –OH, the exposed active Mo sites on MXene can further proceed into a S bond for second adsorption,^[50] whereas the second adsorption in GO is unavailable, leading to inferior LiPSs adsorption–catalysis process than MXene. The introducing of the dual chemical adsorption mode is effective for realizing high adsorption–catalysis property.

As is known to all, a high utilization of MOs catalyst is essential to improve the cell performances. There are two cases for MOs catalysts used in Li–S batteries. The first is MOs serving as sulfur hosts. In this case, the low conductivity and low surface area are the main limitations. The common strategy is to fabricate 3D structures to increase the surface area as well as confining sulfur species, and to improve the conductivity of MOs host by introducing a reduction process step in synthesis or adding carbonaceous additives.^[135] A typical example is the fabrication of 3D ordered macroporous Nb₂O_{5–x} architecture combined with CNTs embedded in the framework to enhance the surface area and conductivity.^[136] After compositing with sulfur by a melting method, the assembled cells could achieve superior performances. Another case is MOs catalysts serving as additives, with carbonaceous materials as sulfur host.^[16,137] MOs are used to decorate the surface of the carbon host, this case is much more common. However, due to the inherent low conductivity of MOs, the LiPSs on MOs will go through an “adsorption–diffusion–conversion” process, in which diffusion is an additional step with sluggish kinetics. Therefore, introducing fine and nanostructured MOs catalyst to shorten the diffusion path is an efficient way to improve the utilization of catalysts. Besides,

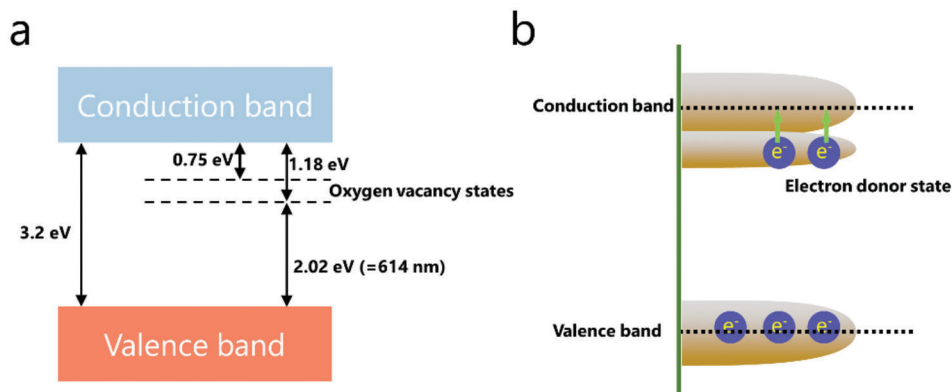


Figure 10. a) A proposed model of band structure of oxygen vacancy state in anatase-TiO₂. b) The overlapping of donor state and conduction band.

changing the conductive properties to directly realize the nucleation of Li₂S upon the MOs surface is also available.^[15a]

No matter if MOs serve as sulfur host or additives, the nanostructured MOs is conducted to the performance for exposing more active sites and physically confining LiPSs. However, the low conductivity and limited catalytic activity still restrict further development and application. To enhance the intrinsic catalytic properties, as well as the side effect by the insulating nature, two main strategies with tuning the basic electron structures are proposed here: 1) constructing oxygen vacancies (OVs) that can improve the conductivity of MOs themselves, as well as enhancing the adsorption and catalytic activity; and 2) by combining another high conductive component to form heterostructures, the nucleation sites could be relocated resulting in a reduced diffusion barrier. In the meanwhile, the formed heterojunction shows a high adsorption–catalytic activity. These two strategies are considered to be effective and will be explained in detail in the following sections.

4. Oxygen Vacancies (OVs) Engineering

4.1. Basic Mechanisms of Oxygen Vacancies in Li-S Chemistry

As discussed above, some MOs (MnO₂, CeO₂, etc.) containing OVs on the surface result in multiple valance states of the M cation, which play a determining role in the catalytic properties. Beyond that, creating rich OVs in bulk MOs is expected to alter the intrinsic electrical conductivity as well as the coordination state toward LiPSs. A typical example is the synthesis of a series of substoichiometric phases Ti_nO_{2n-1} from TiO₂ called Magnéli phases, possessing an improved conductivity with respect to TiO₂. One of its members, Ti₄O₇, even exhibits a metallic conductivity and shows a different sulphophilic surface. Therefore, OVs play a key role in tailoring the catalytic properties, which can modulate intrinsic conductivity, coordination state toward LiPSs, and even influence the mechanism of adsorption–diffusion–catalysis.

In order to figure out the role of OVs in the band structure, pioneering works have contributed to reveal the band changes in the vacancies of TMOs species.^[138] Generally, by removing an oxygen atom from the bulk lattice, the position previously occupied by O²⁻ in the regular lattice would be filled by excess “free” electrons to minimize the formation energy of the vacancy, leading

to localized electrons in the vacancy state.^[138a] Nakamura and co-workers used to proposed a band structure model to understand the localized electrons in anatase TiO₂, where the energy level of the localized donor states of the oxygen vacancy is located 0.75–1.18 eV below the conduction band, as shown in **Figure 10a**.^[138c] On the other hand, the OVs can also cause redistribution of electrons among adjacent metal atoms to form shallow donor states below the conduction band. For anatase it was demonstrated that the energy of these donor states would rise and even overlap with the conduction band at higher vacancy concentration (**Figure 10b**).^[139] As a result, the formation of these electron donor states will result in n-doping, providing an explanation to the enhanced conductivity for rich-OVs MOs. In *d*-band theory, the electron donor states below the conduction band will also influence the *d* band center of the metal atoms that shift toward the Fermi level, which gives rise to a higher adsorption and catalytic activity to LiPSs.

4.2. Synthetic Strategies of Oxygen Vacancies

To construct OVs, thermal treatment of MOs under reducing atmosphere is a common strategy and has been proven to be an effective method. For example, by annealing TiO₂ nanosheets in Ar/H₂ atmosphere at various temperatures, different vacancy concentrations in TiO₂ could be generated.^[140] It is worth noting that the H₂ can also be replaced by other reducing atmospheres like CO, NH₃, CH₄, and so forth.^[139,141] Nevertheless, it is quite challenging to infer how the reduction atmosphere or annealing temperature influences the extent of OVs. In other specific cases, the reducing atmosphere is not even necessary. The oxygen deficient atmosphere (or vacuum) allows the oxygen atom to escape from the MOs lattice, leading to the generation of OVs. For example, by annealing hexagonal WO₃ nanorods in a vacuum environment, monoclinic WO_{3-x} can be obtained by phase transformation.^[142]

Except annealing, OVs can also be introduced by solution methods, using reduction reagents such as NaBH₄, KBH₄, N₂H₄, etc. For example, TiO_{2-x} could be directly obtained by adding TiO₂ nanosheets into a NaBH₄ solution at room temperature.^[143] Compared with the above complicated annealing strategy, the solution method is much more facile. In addition, electrochemical reduction is an alternative green strategy to produce OVs with a

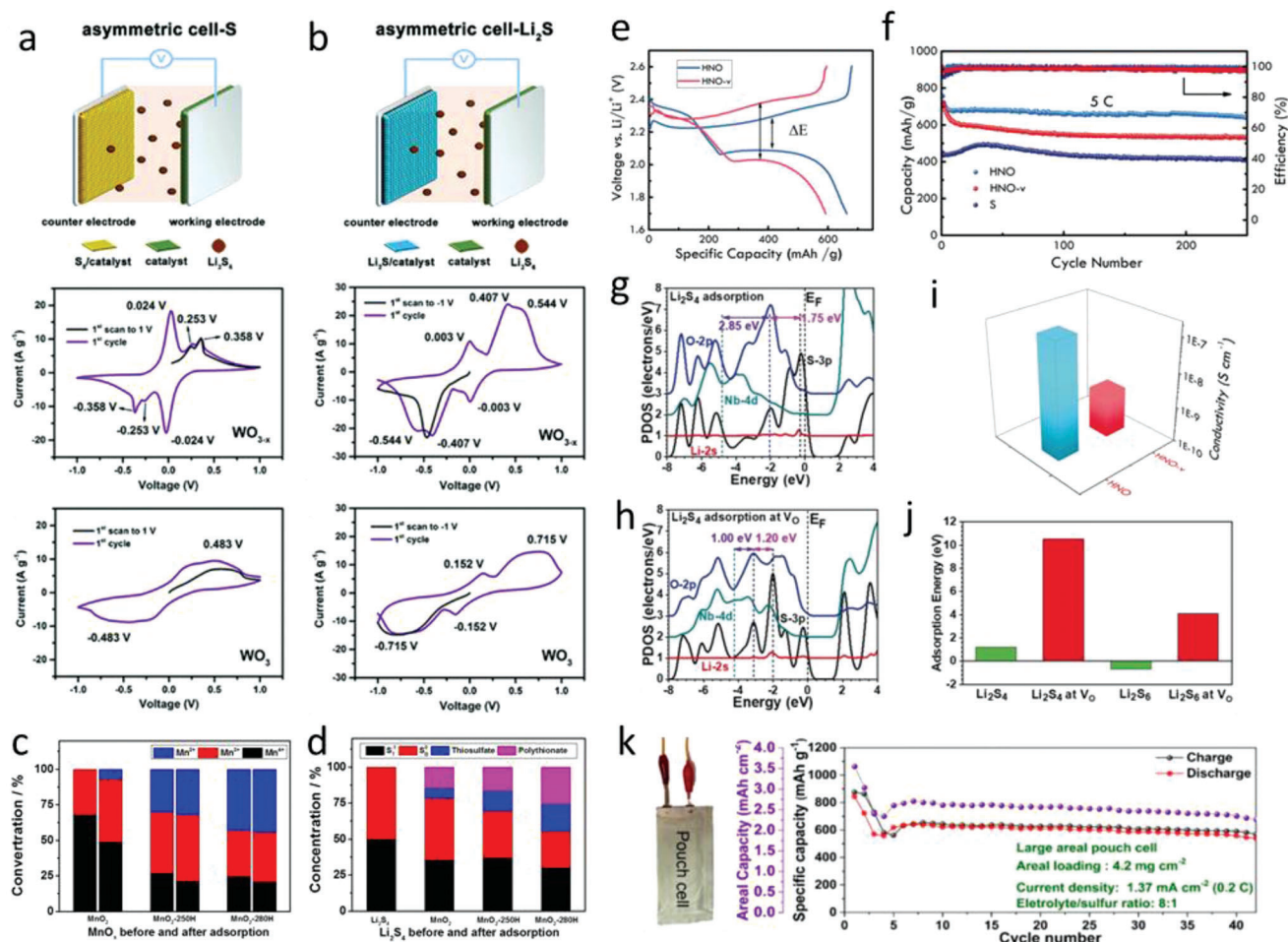


Figure 11. Cyclic voltammograms of asymmetric cell a) -S and b) -Li₂S with WO_{3-x} and WO₃ in Li₂S₆ electrolyte. Reproduced with permission.^[149] Copyright 2018, Wiley-VCH. Comparison of concentration of c) Mn valence states in MnO_x and d) S valence states in Li₂S₄ before and after adsorption. Reproduced with permission.^[151] Copyright 2019, Elsevier. Comparison of e) charge/discharge profile and f) cycling performance of HNO and HNO-v cathode. g, h) The projected density of state (PDOSs) of Li₂S₄ on pristine and OV-HNb₃O₈. i) Electric conductivity and j) adsorption energy to Li₂S₆ of pristine and OV-HNb₃O₈. Reproduced with permission.^[152] Copyright 2019, Wiley-VCH. k) The cycling performance of AOV-Nb₂O_{5-x}@HHPC@S cathode in pouch cell. Reproduced with permission.^[18c] Copyright 2021, Elsevier.

scalable and faster preparation. For instance, the oxygen-deficient TiO_{2-x}, WO_{3-x}, BiVO_{4-x} and ZnO_{1-x} can be fabricated by applying specific potentials to TiO₂, WO₃, BiVO₄ and ZnO in aqueous electrolyte solution.^[144]

Apart from post-treatment of MO, OV can also be created during the synthesis of MO, forming MO_x. By inhibiting nucleation and crystalline growth at the atomic level, defects in the form of vacancies can be generated. Such inhibition processes include solvothermal,^[145] ultrasonication,^[146] ball milling,^[147] and others.^[148] Thus, these MO_x were synthesized by controlling the conversion condition in the process of precursors' transformation.

4.3. Recent Progresses of Oxygen Vacancies in Li-S Chemistry

Up to now, oxygen vacancies in MOs are extensively exploited as active sites for anchoring and catalyzing the redox reactions in Li-S batteries. Since it was first utilized in Li-S chemistry

to suppress the “shuttle effect” and improve the utilization of sulfur through enhancing the adsorption and catalytic activity in 2017,^[143] numerous works were published to demonstrate the effectivity for constructing OVs on MOs in Li-S chemistry. For example, Lee et al. studied the function of OVs in WO_{3-x} nanoplatelets by designing asymmetric cells. As shown in **Figures 11a,b**, in WO_{3-x} and WO₃ based asymmetric cells, the voltammogram of WO_{3-x} based electrodes show higher redox reversibility in both S and Li₂S cells, confirming the bidirectional catalytic properties of OVs in Li-S chemistry.^[149] First principles DFT studies demonstrated that the formation of OVs in anatase TiO₂ enhances the binding energy of polysulfides as well as the electronic conductivity.^[150] To further investigate the behaviors of OVs in the thiosulfate/polythionate formation process, MnO₂ incorporating OVs was synthesized by heating MnO₂ hollow nanospheres under reductive atmosphere.^[151] As shown in **Figure 11c,d**, where OVs-rich MnO₂ present multiple valence states of Mn⁴⁺, Mn³⁺ and Mn²⁺ on the surface, MnO₂ only shows Mn⁴⁺ and Mn³⁺. After adsorption of Li₂S₄, similar redox

behaviors were found where the contribution from Mn^{4+} sites decreases and the one of Mn^{3+} and Mn^{2+} sites increases. The higher thiosulfate/polythionate content in the case of OV-rich MOs indicates accelerated formation of the $\text{S}_2\text{O}_3^{2-}$ mediator, assisting a stronger adsorption of polysulfides as well as their dissociation, corroborating the high catalytic effect of OVs.

However, manufacturing oxygen vacancies is not always beneficial for adsorption and catalytic conversion. An exception was also reported for leading to inferior Li-S performance. As shown Figure 11e,f, after constructing fully oxidized HNb_3O_8 (HNO) and OVs rich HNb_3O_8 (HNO-v) based sulfur electrodes, it can be seen that HNO-v presents a larger polarization and poorer cyclic performance than HNO. Further electronic structure analysis (Figure 11g,h) provided an explanation that the overlap of O $2p_\pi$ and S $3p_\pi$ orbitals in HNO-v induces a strong repulsion between the lone pair of electrons, deteriorating the adsorption-catalytic process. As a result, the OVs rich HNO-v exhibits a decreased electric conductivity as well as a weakened adsorption to LiPSs (Figures 11i,j).^[152] Thus, care should be taken when designing new catalysts using the oxygen vacancy engineering strategy, where the electric conductivity and adsorption are the focusing issues.

By fabricating multifunctional hosts with OVs-rich MOs and structured carbonaceous material, excellent electrochemical performances could be achieved in Li-S batteries. In a recent work, a kind of double shell nanotubes of titanium oxide with OVs in nitrogen-doped carbon host ($\text{OVs-TiO}_{2-x}\text{@NC}$) was prepared, which enabled a super high cycling stability of merely 0.0123% capacity fade per cycle within 3000 cycles at 5 C. When loading an impressively high amount of sulfur (9.5 mg cm^{-2}), a high area capacity of 8.01 mAh cm^{-2} was achieved with a low E/S ratio of $5 \mu\text{L mg}^{-1}$.^[18b] Such superior electrochemical performances can be attributed to the rational integration of physical spatial confinement and high adsorption-catalytic effect of OVs- TiO_{2-x} . Similarly, a multifunctional OVs-niobium oxide electrocatalyst combined with hierarchical porous nanocarbon ($\text{AOV-Nb}_2\text{O}_5\text{-x@HHPC}$) was also fabricated to assess the electrochemical behavior in large area Li-S pouch cells. As shown in Figure 11k, the pouch cell achieved an initial area capacity of 3.54 mAh cm^{-2} and stabilized for more than 40 cycles with sulfur loading of 4.2 mg cm^{-2} at lean electrolyte, which provides a promising application for the future.^[18c] A similar pouch cell performance was also demonstrated in the Nb doped OVs- TiO_{2-x} catalytic sulfur host, the fabricated S-NC@Nb-TiO_{2-x} electrode realized 809 mAh g^{-1} of capacity under 3.5 mg cm^{-2} of sulfur loading and $9.5 \mu\text{L mg}^{-1}$ of E/S ratio.^[59b] Therefore, we note that OVs play important roles in improving the adsorption-catalytic properties thus making it possible to achieve high performance Li-S batteries.

5. Heterostructure Engineering

5.1. Basic Heterostructure Strategies in Li-S Batteries

Heterostructures which consist of two components or blocks forming a heterointerface through physical (mainly van der Waals [vdW] force) or chemical bonds, are an alternative promising strategy to address the insulating issue of MOs. It should be clarified that the heterostructure differs from a general composite

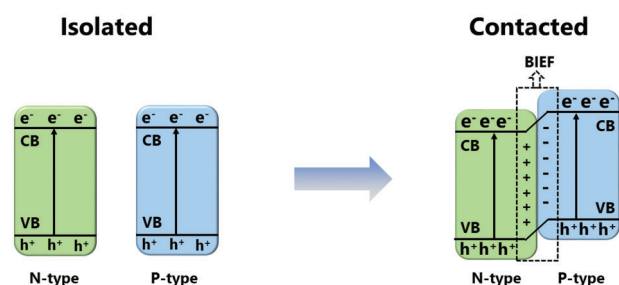


Figure 12. The diagram of formed BIEF after two types of building blocks contact with each other to form a heterojunction.

material that also consists of two different components. The design principle of such a composite material is simply combining the complementary advantages of each component. For instance, MOs with strong LiPSs adsorption are usually combined with a conductive substrate to form a hybrid composite realizing both high adsorption and electron transport properties, while the focus of heterostructures is quite different, mainly on the effect of heterointerface.

Due to the different properties (e.g., band structure, carrier concentration, semiconductor type, Fermi level, alignment style) of building blocks, once brought into contact, the band alignments at the interface proceeds till the Fermi level reaches equilibrium. The band structure of building blocks would be bent resulting in a built-in electric field (BIEF) at the heterointerface (Figure 12). The heterojunction between two components forming the BIEF are revealed to specifically facilitate adsorption and reduction/oxidation reactions of redox species.^[153] For example, Sun et al. designed a kind of Mott-Schottky heterojunction and investigated the potential catalytic activity in Li-S chemistry. They found that the BIEF with negatively and positively charged interfaces can strongly adsorb Li^+ and polysulfide anions of LiPSs, respectively, thus lowering the energy barriers of sulfur redox reactions and accelerating catalytic conversion.^[154] The resulting heterostructure provides both the sum of the contribution of the individual components and the heteroconjunction at their interface with completely improved properties, realizing a performance superior to the sum of its part (" $1+1>2$ ").

5.2. Synthesis Strategies of MO Based Heterostructures

Different from physically mixing of two components, heterostructures are formed with conjunction between the two blocks guaranteeing the close contact. To realize this, partial sulfuration, reduction, or nitrification has attracted much attention. To take an example, as shown in Figure 13a, a type of $\text{WS}_2\text{-WO}_3$ heterostructure was reported by in situ sulfuration of WO_3 . By controlling the weight ratio and annealing temperature, an adjustable constituent ratio of $\text{WS}_2\text{-WO}_3$ heterostructure could be obtained.^[155] Another typical example is the synthesis of the MOs-MXene heterostructure by partial oxidation of MXene. When treating $\text{Ti}_3\text{C}_2\text{T}_x$ (T is a terminal as functional groups) by a hydrothermal process, TiO_2 nanoparticles were nucleated on the surface of $\text{Ti}_3\text{C}_2\text{T}_x$ to form a $\text{TiO}_2\text{-Ti}_3\text{C}_2\text{T}_x$ heterostructure.^[156] Similarly, a $\text{Nb}_2\text{O}_5\text{-NbC}_3\text{T}_x$ heterostructure was also reported with Nb_2O_5 nanoparticles uniformly distributed on the surface of

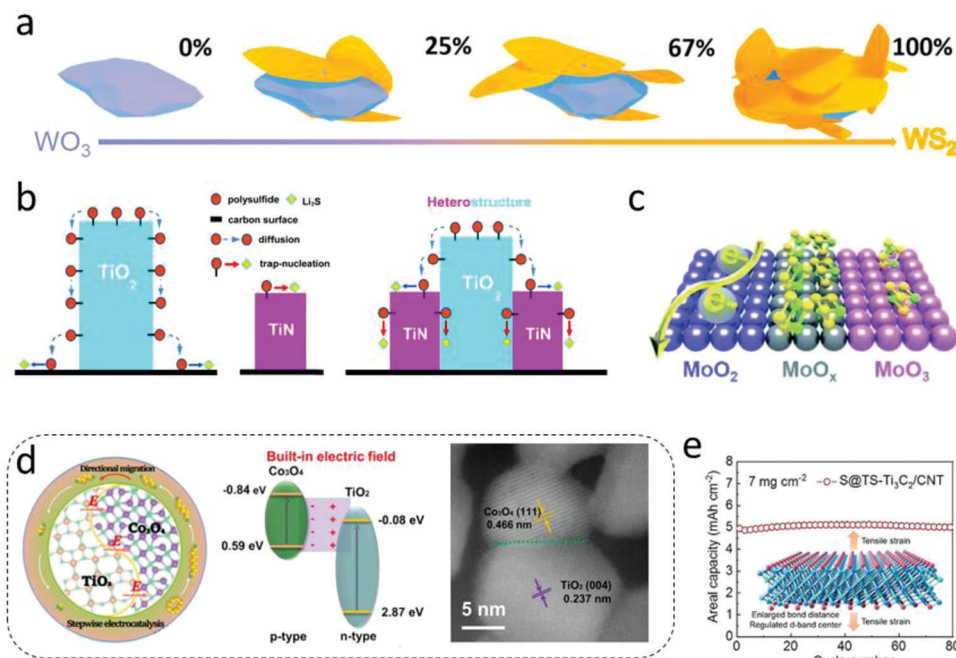


Figure 13. a) The illustration of component change with different sulfurization degree. Reproduced with permission.^[155] Copyright 2020, Wiley-VCH. b) Schematic of principle of LiPSs conversion process on TiO₂-TiN heterostructure. Reproduced with permission.^[15b] Copyright 2017, Royal Society of Chemistry. c) Schematic of MoO₃/MoO₂ heterostructure with a MoO_x transition state. Reproduced with permission.^[103] Copyright 2020, Royal Society of Chemistry. d) Schematic diagram of Co₃O₄ and TiO₂ heterostructure with BIEF. Reproduced with permission.^[77] Copyright 2021, Wiley-VCH. e) Illustration and the high loading performance of S@TS-Ti₃C₂/CNT. Reproduced with permission.^[160] Copyright 2021, Wiley-VCH.

NbC₃T_x by heating Nb₄C₃T_x in CO₂ flow.^[157] In addition, other methods like atomic layer deposition (ALD), chemical vapor deposition (CVD), and so on can also produce a heterostructure material with one component onto a target substrate.^[158]

Aside from above strategies, heterostructure material can also be synthesized through a one step process such as annealing or hydrothermal treatment. And the resulting product can be controlled by the ratio of reactants or the reaction conditions. For example, a TiO₂-TiN heterostructure was synthesized by the reaction between urea and TiCl₄ annealed under N₂ atmosphere, where the resulting product can be determined by the molar ratio of urea/TiCl₄. When the ratio was between 2:1 and 10:1, the TiO₂-TiN heterostructure can be obtained.^[15b] Another example is the MoO₂/α-MoC heterostructure constructed by the thermal decomposition of Mo₃O₁₀(C₆H₈N)₂·2H₂O in Ar atmosphere where the resulting product is temperature dependent. Annealing temperatures of 600 and 700 °C would result in pure MoO₂ and α-MoC, respectively. Thus, MoO₂/α-MoC heterostructures can be obtained when the temperature was set at 650 °C.^[159]

5.3. Recent Progresses of MO Based Heterostructures in Li-S Chemistry

In a typical adsorption-diffusion-conversion process of LiPSs in MO based electrocatalysts, LiPSs must diffuse from nonconductive metal oxide to the conductive carbon surface to realize further conversion. This process always shows slow reaction kinetics. Aiming to solve this problem, the concept of heterostructure was

initially introduced by Yang's group in Li-S chemistry to smooth such diffusion-conversion process.^[15b] As shown in Figure 13b, they combined highly polar TiO₂ and highly conductive TiN to design a twinborn TiO₂-TiN heterostructure loaded on graphene. Comparing with bare TiO₂ that has a long diffusion path from the TiO₂ surface to the nearby carbon substrate, the LiPSs can quickly diffuse to nearby TiN for further conversion after being trapped at the TiO₂ surface. As a result, the performances of TiO₂-TiN heterostructures were much better than both pure TiO₂ and TiN, realizing a high sulfur loading performance of 4.3 mg cm⁻² and a capacity retention of 67% over 2000 cycles at 1C.

Based on the above concept of combining desired properties to smooth the diffusion of LiPSs, the heterostructure combining metal oxide and metal carbide/nitride/sulfate/phosphide was proposed with the polar character of the former and outstanding catalytic activity of the latter.^[161] We note that the formed heterojunction can provide a higher adsorption and catalytic activity. For example, in a typical Mn₃O₄-MnPx heterostructure, the electron redistribution at the interface between Mn₃O₄ and MnPx would lead to the electron accumulation on P atoms. Thus, the Mn can easily accept electrons from LiPSs, displaying a more optimal binding energy and a high catalytic activity.^[162] Besides sharp interfaces that are present at most heterojunctions, the conjunction could also showcase a transition state. As shown in Figure 13c, the conjunction in the MoO₃/MoO₂ heterostructure exhibits a unique transition state of MoO_x formed between the MoO₃ and MoO₂, which provides a stronger adsorption of LiPSs as compared to MoO₃ and MoO₂. This enables Li-S batteries with a high stable cycling performance and a capacity decay of 0.02% per cycle over 850 cycles.^[103]

As stated above, the heterostructure endows the redistribution of electrons, leading to the formation of BIEF with electric positive and negative charged sides, which shows impressively adsorption and redox activity of LiPSs.^[154] Beyond that, the BIEF can also spatially propel the stepwise conversion. Zhang et al. implemented p-n heterojunctions by combining n-type TiO₂ and p-type Co₃O₄ and found that the BIEF formed at their interface could induce the directional migration of negatively charged polysulfides from p-type Co₃O₄ to n-type TiO₂, realizing a spatially optimized distribution of LiPSs (Figure 13d).^[77] Bridged by the BIEF of p-n heterojunctions, the interfacial architecture with distinct catalysis could synergistically improve the Li-S performance by spatially enhancing the stepwise conversion of LiPSs. That is, the high catalytic Co₃O₄ ensures the precise conversion from S₈ to Li₂S₄, and TiO₂ can strongly anchor Li₂S₄ and further mediate the effective nucleation. As a result, a capacity of 5.5 mAh cm⁻² could be achieved at the sulfur loading of 5.5 mg cm⁻² and E/S ratio of 8 μ L mg⁻¹. Except the effect of BIEF in the heterojunction, the imposed tensile strain in the heterojunction also has great effect to the polysulfide behavior. Chen et al. investigated the exerted internal stress on the MXene (Ti₃C₂T_x) after in-situ spraying of an oxidation layer, and found the formed O-Ti-C in the interface exerts a lattice distortion and enlarge the T-Ti bond of Ti₃C₂, resulting in upshift of *d*-band center of facial Ti atom closer to Fermi level, which strengthened the adsorption and catalytic conversion to LiPSs. After interwoven with CNTs, the hierarchical architecture achieved a high area capacity of 5 mAh cm⁻² with high sulfur loading of 7 mg cm⁻² and lean E/S ratio (Figure 13e).^[160]

The heterostructure which combines the advantages of adsorption and catalytic superiority can smooth the LiPSs diffusion in the typical “adsorption-diffusion-conversion” process, significantly improving the transfer kinetics in Li-S batteries. Nevertheless, the influence of charge redistribution and other effect in the heteroconjunction is still a matter of investigation. Further development is still needed to elucidate the systematic nature and underlying mechanism of heterojunctions in future research.

6. Conclusion and Outlook

To summarize, in this review, we have comprehensively discussed the underlying adsorption and catalytic mechanism of LiPSs in Li-S chemistry. We note that the catalytic property is correlated with the adsorption behavior rather than being independent each other. In this respect, three types of interactions of polysulfide including Li bond, S bond and sulfur-chain catenation are classified. Especially, we highlight the significance of orbital hybridization which plays an important role in further catalytic analysis. Although the precise mechanism governing the catalytic activity still remains unclear, the Sabatier principle, *d*-band theory, *d-p* model and Goldilocks principles are introduced here, respectively, which provide valuable guidance for material screening and rational electrocatalysts design.

MOs stand out among metal compounds for their high chemical stability and low cost. There are also other metal compounds that can provide strong and effective affinity to LiPSs, such as metal carbides, sulfides, nitrides and phosphides. However, the above metal compounds usually require strict conditions for synthesis to avoid oxidation, such as high purity of inert atmosphere

and high temperature, but still face uncontrollable surface oxidation after being exposed with air.^[163] It is interesting to note that MOs can also serve as precursor to synthesize above mentioned four metal compounds.^[12,41] Thus, MOs oxides with high stability and low cost are most promising for applications in Li-S batteries. Moreover, since the exposed surface of MOs is responsible for anchoring, diffusion and catalytic reaction of LiPSs, the nanostructured MOs with controllable exposed surfaces are expected to afford efficient and effective anchoring sites for LiPSs.

Next, different nanostructured MOs based conductive composites applied in Li-S batteries are reviewed. It is found that: 1) most MOs with oxygen termination are able to provide lone pair electrons to form a Li bonds with LiPSs. But some MOs with non-stoichiometric metal centers present sulfophilic surfaces, which are inclined to form S bonds; 2) besides chemical composition, different bulk phases and crystal facets can also deliver different adsorption and catalytic activities; and 3) the dual chemical adsorption mode combining both sulfur-chain catenation and Li/S bond mechanism favors to realize significant adsorption and catalytic properties. In addition, to overcome the sluggish diffusion step in typical “adsorption-diffusion-conversion” processes and the low conductivity nature of MOs, constructing OV and heterostructure are the two main strategies by altering the electronic structure. With many promising accomplishments being achieved, these two strategies showcase potential for the design of high performance Li-S batteries of commercial interest.

Indeed, the change of the electronic structure especially valance state of the catalytic material can regulate the catalytic activity thus making a significant influence on the electrocatalyst's performance. *D*-band theory provides an explanation that the electron structure influences catalytic activity by shifting the relative position of *d*-band center. Manufacturing defects, including vacancies, disorders, distortions, boundaries, single atoms, etc., are the common strategies to tune electron structure and further influences the catalytic performance. In the future, controllable tuning of the electronic structures of catalysts, is of crucial importance to realize highly active and efficient catalysts. As such, MOs, with high chemical stability, are most promising and preferable.

Overall, challenges need to be overcome to develop a highly efficient multifunctional catalytic material to realize a high performance that meets the practical requirement. MOs being cost-efficient, durable, highly polar, environmentally friendly, and possessing tunable properties have the potential to serve as promising catalytic material for the ultimate practical application of high energy density Li-S batteries.

Acknowledgements

The authors acknowledge funding from the Swiss National Science Foundation via the Southeast Asia-Europe Joint Funding Scheme 2020 (IZFZ2_202476) and Empa internal research grants (Empa-IRC-2019 Supercap, IRC-2020 NitfixMX). The authors gratefully acknowledge Frank Nüesch for his useful discussions and corrections to the manuscript.

Conflict of Interest

The authors declare no conflict of interest.

Keywords

catalytic conversion, heterostructure, lithium-sulfur batteries, metal oxides, polysulfide shuttle

Received: September 29, 2022

Revised: November 10, 2022

Published online: December 11, 2022

- [1] a) W. M. Kang, N. P. Deng, J. G. Ju, Q. X. Li, D. Y. Wu, X. M. Ma, L. Li, M. Naebe, B. W. Cheng, *Nanoscale* **2016**, *8*, 16541; b) R. Kumar, J. Liu, J. Y. Hwang, Y. K. Sun, *J. Mater. Chem. A* **2018**, *6*, 11582; c) A. Manthiram, Y. Z. Fu, Y. S. Su, *Acc. Chem. Res.* **2013**, *46*, 1125.
- [2] a) P. Wang, B. J. Xi, M. Huang, W. H. Chen, J. K. Feng, S. L. Xiong, *Adv. Energy Mater.* **2021**, *11*, 2002893; b) Y. Yang, G. Y. Zheng, Y. Cui, *Chem. Soc. Rev.* **2013**, *42*, 3018.
- [3] R. G. Cao, W. Xu, D. P. Lv, J. Xiao, J. G. Zhang, *Adv. Energy Mater.* **2015**, *5*, 1402273.
- [4] a) X. L. Ji, L. F. Nazar, *J. Mater. Chem.* **2010**, *20*, 9821; b) A. Manthiram, Y. Z. Fu, S. H. Chung, C. X. Zu, Y. S. Su, *Chem. Rev.* **2014**, *114*, 11751; c) B. Scrosati, J. Garche, *J. Power Sources* **2010**, *195*, 2419.
- [5] a) N. Jayaprakash, J. Shen, S. S. Moganty, A. Corona, L. A. Archer, *Angew. Chem., Int. Ed.* **2011**, *50*, 5904; b) X. L. Ji, K. T. Lee, L. F. Nazar, *Nat. Mater.* **2009**, *8*, 500; c) J. C. Guo, Y. H. Xu, C. S. Wang, *Nano Lett.* **2011**, *11*, 4288; d) B. Zhang, X. Qin, G. R. Li, X. P. Gao, *Energy Environ. Sci.* **2010**, *3*, 1531; e) G. Y. Zheng, Y. Yang, J. J. Cha, S. S. Hong, Y. Cui, *Nano Lett.* **2011**, *11*, 4462.
- [6] a) L. B. Ma, R. P. Chen, G. Y. Zhu, Y. Hu, Y. R. Wang, T. Chen, J. Liu, Z. Jin, *ACS Nano* **2017**, *11*, 7274; b) G. M. Zhou, Y. B. Zhao, A. Manthiram, *Adv. Energy Mater.* **2015**, *5*, 1402263.
- [7] a) N. Kang, Y. X. Lin, L. Yang, D. P. Lu, J. Xiao, Y. Qi, M. Cai, *Nat. Commun.* **2019**, *10*, 4597; b) W. J. Xue, Z. Shi, L. M. Suo, C. Wang, Z. A. Wang, H. Z. Wang, K. P. So, A. Maurano, D. W. Yu, Y. M. Chen, L. Qie, Z. Zhu, G. Y. Xu, J. Kong, J. Li, *Nat. Energy* **2019**, *4*, 374.
- [8] S. Dorfler, H. Althues, P. Hartel, T. Abendroth, B. Schumm, S. Kaskel, *Joule* **2020**, *4*, 539.
- [9] a) R. Wang, J. L. Yang, X. Chen, Y. Zhao, W. G. Zhao, G. Y. Qian, S. N. Li, Y. G. Xiao, H. Chen, Y. S. Ye, G. M. Zhou, F. Pan, *Adv. Energy Mater.* **2020**, *10*, 1903550; b) Z. H. Li, C. Zhou, J. H. Hua, X. F. Hong, C. L. Sun, H. W. Li, X. Xu, L. Q. Mai, *Adv. Mater.* **2020**, *32*, 1907444; c) P. Y. Li, H. W. Lv, Z. L. Li, X. P. Meng, Z. Lin, R. H. Wang, X. J. Li, *Adv. Mater.* **2021**, *33*, 2007803; d) D. Luo, C. J. Li, Y. G. Zhang, Q. Y. Ma, C. Y. Ma, Y. H. Nie, M. Li, X. F. Weng, R. Huang, Y. Zhao, L. L. Shui, X. Wang, Z. W. Chen, *Adv. Mater.* **2022**, *34*, 2105541.
- [10] a) Z. Z. Du, X. J. Chen, W. Hu, C. H. Chuang, S. Xie, A. J. Hu, W. S. Yan, X. H. Kong, X. J. Wu, H. X. Ji, L. J. Wan, *J. Am. Chem. Soc.* **2019**, *141*, 3977; b) Y. X. Ren, T. S. Zhao, M. Liu, P. Tan, Y. K. Zeng, *J. Power Sources* **2016**, *336*, 115.
- [11] a) X. Luo, X. B. Lu, X. D. Chen, Y. Chen, C. Y. Yu, D. W. Su, G. X. Wang, L. F. Cui, *J. Energy Chem.* **2020**, *50*, 63; b) X. Y. Tao, J. G. Wang, C. Liu, H. T. Wang, H. B. Yao, G. Y. Zheng, Z. W. Seh, Q. X. Cai, W. Y. Li, G. M. Zhou, C. X. Zu, Y. Cui, *Nat. Commun.* **2016**, *7*, 11203; c) Y. Y. Mao, G. R. Li, Y. Guo, Z. P. Li, C. D. Liang, X. S. Peng, Z. Lin, *Nat. Commun.* **2017**, *8*, 14628; d) J. Balach, J. Linnemann, T. Jaumann, L. Giebel, *J. Mater. Chem. A* **2018**, *6*, 23127.
- [12] J. B. Zhou, X. J. Liu, L. Q. Zhu, J. Zhou, Y. Guan, L. Chen, S. W. Niu, J. Y. Cai, D. Sun, Y. C. Zhu, J. Du, G. M. Wang, Y. T. Qian, *Joule* **2018**, *2*, 2681.
- [13] S. Feng, Z. H. Fu, X. Chen, Q. Zhang, *Informat* **2022**, *4*, e12304.
- [14] X. Liu, J. Q. Huang, Q. Zhang, L. Q. Mai, *Adv. Mater.* **2017**, *29*, 1601759.
- [15] a) H. J. Peng, G. Zhang, X. Chen, Z. W. Zhang, W. T. Xu, J. Q. Huang, Q. Zhang, *Angew. Chem., Int. Ed.* **2016**, *55*, 12990; b) T. H. Zhou, W. Lv, J. Li, G. M. Zhou, Y. Zhao, S. X. Fan, B. L. Liu, B. H. Li, F. Y. Kang, Q. H. Yang, *Energy Environ. Sci.* **2017**, *10*, 1694.
- [16] Y. K. Wang, R. F. Zhang, J. Chen, H. Wu, S. Y. Lu, K. Wang, H. L. Li, C. J. Harris, K. Xi, R. V. Kumar, S. J. Ding, *Adv. Energy Mater.* **2019**, *9*, 1900953.
- [17] a) Y. K. Wang, R. F. Zhang, Z. H. Sun, H. Wu, S. Y. Lu, J. N. Wang, W. Yu, J. M. Liu, G. X. Gao, S. J. Ding, *Adv. Mater. Interfaces* **2020**, *7*, 1902092; b) D. R. Wang, D. Luo, Y. G. Zhang, Y. Zhao, G. F. Zhou, L. L. Shui, Z. W. Chen, X. Wang, *Nano Energy* **2021**, *81*, 105602.
- [18] a) Z. Zhang, D. Luo, G. R. Li, R. Gao, M. Li, S. Li, L. Zhao, H. Z. Dou, G. B. Wen, S. Sy, Y. F. Hu, J. D. Li, A. P. Yu, Z. W. Chen, *Matter* **2020**, *3*, 920; b) W. Q. Yao, W. Z. Zheng, K. Han, S. X. Xiao, *J. Mater. Chem. A* **2020**, *8*, 19028; c) S. Cheng, J. Wang, S. R. Duan, J. Zhang, Q. Wang, Y. Zhang, L. G. Li, H. T. Liu, Q. B. Xiao, H. Z. Lin, *Chem. Eng. J.* **2021**, *417*, 128172; d) L. L. Ma, L. J. Yu, J. C. Liu, Y. Q. Su, S. Li, X. H. Zang, T. Meng, S. H. Zhang, J. J. Song, J. Y. Wang, X. X. Zhao, Z. M. Cui, N. Wang, Y. Zhao, *Energy Storage Mater.* **2022**, *44*, 180; e) W. T. Qi, W. C. Yi, W. Jiang, R. Ling, C. Yang, S. D. Liu, S. C. Jun, Y. Yamauchi, B. Q. Cao, *ACS Sustainable Chem. Eng.* **2021**, *9*, 14451.
- [19] H. L. Pan, X. L. Wei, W. A. Henderson, Y. Y. Shao, J. Z. Chen, P. Bhat-tacharya, J. Xiao, J. Liu, *Adv. Energy Mater.* **2015**, *5*, 1500113.
- [20] L. C. Yin, J. Liang, G. M. Zhou, F. Li, R. Saito, H. M. Cheng, *Nano Energy* **2016**, *25*, 203.
- [21] a) Q. F. Zhang, Y. P. Wang, Z. W. Seh, Z. H. Fu, R. F. Zhang, Y. Cui, *Nano Lett.* **2015**, *15*, 3780; b) Q. Pang, X. Liang, C. Y. Kwok, L. F. Nazar, *Nat. Energy* **2016**, *1*, 16132.
- [22] a) Z. W. Seh, Q. F. Zhang, W. Y. Li, G. Y. Zheng, H. B. Yao, Y. Cui, *Chem. Sci.* **2013**, *4*, 3673; b) T. Z. Hou, X. Chen, H. J. Peng, J. Q. Huang, B. Q. Li, Q. Zhang, B. Li, *Small* **2016**, *12*, 3283; c) X. Y. Tao, J. G. Wang, C. Liu, H. T. Wang, H. B. Yao, G. Y. Zheng, Z. W. Seh, Q. X. Cai, W. Y. Li, G. M. Zhou, C. X. Zu, Y. Cui, *Nat. Commun.* **2016**, *7*, 11203; d) J. M. Zheng, J. Tian, D. X. Wu, M. Gu, W. Xu, C. M. Wang, F. Gao, M. H. Engelhard, J. G. Zhang, J. Liu, J. Xiao, *Nano Lett.* **2014**, *14*, 2345.
- [23] H. Margenau, *Rev. Mod. Phys.* **1939**, *11*, 1.
- [24] a) J. X. Song, M. L. Gordin, T. Xu, S. R. Chen, Z. X. Yu, H. Sohn, J. Lu, Y. Ren, Y. H. Duan, D. H. Wang, *Angew. Chem., Int. Ed.* **2015**, *54*, 4325; b) T. Z. Hou, W. T. Xu, X. Chen, H. J. Peng, J. Q. Huang, Q. Zhang, *Angew. Chem., Int. Ed.* **2017**, *56*, 8178.
- [25] D. N. Shigorin, *Spectrochim. Acta* **1959**, *14*, 198.
- [26] A. B. Sannigrahi, T. Kar, B. G. Niyogi, P. Hobza, P. v. R. Schleyer, *Chem. Rev.* **1990**, *90*, 1061.
- [27] R. G. Pearson, *J. Chem. Educ.* **1968**, *45*, 643.
- [28] X. Chen, H. J. Peng, R. Zhang, T. Z. Hou, J. Q. Huang, B. Li, Q. Zhang, *ACS Energy Lett.* **2017**, *2*, 795.
- [29] Q. Pang, X. Liang, C. Y. Kwok, L. F. Nazar, *J. Electrochem. Soc.* **2015**, *162*, A2567.
- [30] Z. Y. Han, S. Y. Zhao, J. W. Xiao, X. W. Zhong, J. Z. Sheng, W. Lv, Q. F. Zhang, G. M. Zhou, H. M. Cheng, *Adv. Mater.* **2021**, *33*, 2105947.
- [31] S. S. Zhang, *Electrochim. Acta* **2012**, *70*, 344.
- [32] L. L. Peng, Z. Y. Wei, C. Z. Wan, J. Li, Z. Chen, D. Zhu, D. Baumann, H. T. Liu, C. S. Allen, X. Xu, A. I. Kirkland, I. Shakir, Z. Almutairi, S. Tolbert, B. Dunn, Y. Huang, P. Sautet, X. F. Duan, *Nat. Catal.* **2020**, *3*, 762.
- [33] a) Q. Pang, C. Y. Kwok, D. Kundu, X. Liang, L. F. Nazar, *Joule* **2019**, *3*, 136; b) G. Zhang, Z. W. Zhang, H. J. Peng, J. Q. Huang, Q. Zhang, *Small Methods* **2017**, *1*, 1700134.
- [34] a) Y. W. Wang, W. J. Qiu, E. H. Song, F. Gu, Z. H. Zheng, X. L. Zhao, Y. Q. Zhao, J. J. Liu, W. Q. Zhang, *Natl. Sci. Rev.* **2018**, *5*, 327; b) S. L. Jiao, X. W. Fu, H. W. Huang, *Adv. Funct. Mater.* **2022**, *32*, 2107651.
- [35] a) T. G. Jeong, D. S. Choi, H. Song, J. Choi, S. A. Park, S. H. Oh, H. Kim, Y. Jung, Y. T. Kim, *ACS Energy Lett.* **2017**, *2*, 327; b) Z. Y. Han,

- R. H. Gao, Y. Y. Jia, M. T. Zhang, Z. J. Lao, B. Chen, Q. Zhang, C. Li, W. Lv, G. M. Zhou, *Mater. Today* **2022**, 57, 84.
- [36] a) A. J. Medford, A. Vojvodic, J. S. Hummelshøj, J. Voss, F. Abild-Pedersen, F. Studt, T. Bligaard, A. Nilsson, J. K. Nørskov, *J. Catal.* **2015**, 328, 36; b) H. Toulhoat, P. Raybaud, S. Kasztelan, G. Kresse, J. Hafner, *Catal. Today* **1999**, 50, 629; c) L. Wang, G. R. Li, S. Liu, X. P. Gao, *Adv. Funct. Mater.* **2021**, 31, 2010693.
- [37] a) B. Hammer, J. K. Nørskov, *Nature* **1995**, 376, 238; b) A. Nilsson, L. G. M. Pettersson, B. Hammer, T. Bligaard, C. H. Christensen, J. K. Nørskov, *Catal. Lett.* **2005**, 100, 111.
- [38] a) Z. H. Shen, Z. L. Zhang, M. Li, Y. F. Yuan, Y. Zhao, S. Zhang, C. L. Zhong, J. Zhu, J. Lu, H. G. Zhang, *ACS Nano* **2020**, 14, 6673; b) Z. H. Shen, M. Q. Cao, Z. L. Zhang, J. Pu, C. L. Zhong, J. C. Li, H. X. Ma, F. J. Li, J. Zhu, F. Pan, H. G. Zhang, *Adv. Funct. Mater.* **2020**, 30, 1906661; c) Z. X. Liu, P. B. Balbuena, P. P. Mukherjee, *J. Phys. Chem. Lett.* **2017**, 8, 1324.
- [39] P. Zeng, C. Liu, C. Cheng, C. Yuan, K. H. Dai, J. Mao, L. R. Zheng, J. Zhang, L. Y. Chang, S. C. Haw, T. S. Chan, H. P. Lin, L. Zhang, *J. Mater. Chem. A* **2021**, 9, 18526.
- [40] Z. X. Shi, M. Li, J. Y. Sun, Z. W. Chen, *Adv. Energy Mater.* **2021**, 11, 2100332.
- [41] J. D. Shen, X. J. Xu, J. Liu, Z. B. Liu, F. K. Li, R. Z. Hu, J. W. Liu, X. H. Hou, Y. Z. Feng, Y. Yu, M. Zhu, *ACS Nano* **2019**, 13, 8986.
- [42] a) Z. X. Zhao, Z. L. Yi, H. J. Li, R. Pathak, Z. W. Yang, X. M. Wang, Q. Q. Qiao, *Nano Energy* **2021**, 81, 105621; b) J. D. Shen, X. J. Xu, J. Liu, Z. S. Wang, S. Y. Zuo, Z. B. Liu, D. C. Zhang, J. W. Liu, M. Zhu, *Adv. Energy Mater.* **2021**, 11, 2100673.
- [43] Q. Cheng, W. H. Xu, S. Y. Qin, S. Das, T. W. Jin, A. J. Li, A. C. Li, B. Y. Qie, P. C. Yao, H. W. Zhai, C. M. Shi, X. Yong, Y. Yang, *Angew. Chem., Int. Ed.* **2019**, 58, 5557.
- [44] H. L. Ye, J. G. Sun, S. L. Zhang, T. R. Zhang, Y. Zhao, C. Y. Song, Q. F. Yao, J. Y. Lee, *Chem. Eng. J.* **2021**, 410, 128284.
- [45] a) M. Zhao, H. J. Peng, J. Y. Wei, J. Q. Huang, B. Q. Li, H. Yuan, Q. Zhang, *Small Methods* **2020**, 4, 1900344; b) J. Xie, H. J. Peng, Y. W. Song, B. Q. Li, Y. Xiao, M. Zhao, H. Yuan, J. Q. Huang, Q. Zhang, *Angew. Chem., Int. Ed.* **2020**, 59, 17670; c) M. Zhao, X. Chen, X. Y. Li, B. Q. Li, J. Q. Huang, *Adv. Mater.* **2021**, 33, 2007298.
- [46] F. Y. Fan, W. C. Carter, Y. M. Chiang, *Adv. Mater.* **2015**, 27, 5203.
- [47] Z. Lin, Z. C. Liu, W. J. Fu, N. J. Dudney, C. D. Liang, *Angew. Chem., Int. Ed.* **2013**, 52, 7460.
- [48] X. Liang, C. Hart, Q. Pang, A. Garsuch, T. Weiss, L. F. Nazar, *Nat. Commun.* **2015**, 6, 5682.
- [49] H. Stamm, H. Wintzer, *Ber. Dtsch. Chem. Ges.* **1938**, 71, 2212.
- [50] X. Liang, Y. Rongom, C. Y. Kwok, Q. Pang, L. F. Nazar, *Adv. Mater.* **2017**, 29, 1603040.
- [51] a) X. Liang, C. Y. Kwok, F. Lodi-Marzano, Q. Pang, M. Cuisinier, H. Huang, C. J. Hart, D. Houtarde, K. Kaup, H. Sommer, T. Brezesinski, J. Janek, L. F. Nazar, *Adv. Energy Mater.* **2016**, 6, 1501636; b) H. Tang, W. L. Li, L. M. Pan, C. P. Cullen, Y. Liu, A. Pakdel, D. H. Long, J. Yang, N. McEvoy, G. S. Duesberg, V. Nicolosi, C. F. Zhang, *Adv. Sci.* **2018**, 5, 1800502; c) H. J. Kang, J. W. Park, H. J. Hwang, H. Kim, K. S. Jang, X. L. Ji, H. J. Kim, W. B. Im, Y. S. Jun, *Carbon Energy* **2021**, 3, 976; d) T. P. Zhang, F. Y. Hu, W. L. Shao, S. Y. Liu, H. Peng, Z. H. Song, C. Song, N. Li, X. G. Jian, *ACS Nano* **2021**, 15, 15027.
- [52] H. Tang, W. L. Li, L. M. Pan, K. J. Tu, F. Du, T. Qiu, J. Yang, C. P. Cullen, N. McEvoy, C. F. Zhang, *Adv. Funct. Mater.* **2019**, 29, 1901907.
- [53] Y. Chen, T. Y. Wang, H. J. Tian, D. W. Su, Q. Zhang, G. X. Wang, *Adv. Mater.* **2021**, 33, 2003666.
- [54] J. C. Vedrine, *Catalysts* **2017**, 7, 341.
- [55] Y. J. Choi, B. S. Jung, D. J. Lee, J. H. Jeong, K. W. Kim, H. J. Ahn, K. K. Cho, H. B. Gu, *Phys. Scr.* **2007**, T129, 62.
- [56] X. L. Ji, S. Evers, R. Black, L. F. Nazar, *Nat. Commun.* **2011**, 2, 325.
- [57] M. S. Song, S. C. Han, H. S. Kim, J. H. Kim, K. T. Kim, Y. M. Kang, H. J. Ahn, S. X. Dou, J. Y. Lee, *J. Electrochem. Soc.* **2004**, 151, A791.
- [58] S. Evers, T. Yim, L. F. Nazar, *J. Phys. Chem. C* **2012**, 116, 19653.
- [59] a) X. Song, T. Gao, S. Q. Wang, Y. Bao, G. P. Chen, L. X. Ding, H. H. Wang, *J. Power Sources* **2017**, 356, 172; b) Z. K. He, T. T. Wan, Y. H. Luo, G. H. Liu, L. L. Wu, F. Li, Z. S. Zhang, G. R. Li, Y. G. Zhang, *Chem. Eng. J.* **2022**, 448, 137656.
- [60] N. Ding, L. Zhou, C. W. Zhou, D. S. Geng, J. Yang, S. W. Chien, Z. L. Liu, M. F. Ng, A. S. Yu, T. S. A. Hor, M. B. Sullivan, Y. Zong, *Sci. Rep.* **2016**, 6, 33154.
- [61] B. Ding, G. Y. Xu, L. F. Shen, P. Nie, P. F. Hu, H. Dou, X. G. Zhang, *J. Mater. Chem. A* **2013**, 1, 14280.
- [62] Z. Zhang, Q. Li, K. Zhang, W. Chen, Y. Q. Lai, J. Li, *J. Power Sources* **2015**, 290, 159.
- [63] Z. B. Xiao, Z. Yang, L. Wang, H. G. Nie, M. E. Zhong, Q. Q. Lai, X. J. Xu, L. J. Zhang, S. M. Huang, *Adv. Mater.* **2015**, 27, 2891.
- [64] Z. Zhang, Q. Li, S. F. Jiang, K. Zhang, Y. Q. Lai, J. Li, *Chem. - Eur. J.* **2015**, 21, 1343.
- [65] W. J. Xue, Q. B. Yan, G. Y. Xu, L. M. Suo, Y. M. Chen, C. Wang, C. A. Wang, J. Li, *Nano Energy* **2017**, 38, 12.
- [66] L. Q. Yang, G. C. Li, X. Jiang, T. R. Zhang, H. B. Lin, J. Y. Lee, *J. Mater. Chem. A* **2017**, 5, 12506.
- [67] M. M. Fang, Z. M. Chen, Y. Liu, J. P. Quan, C. Yang, L. C. Zhu, Q. B. Xu, Q. Xu, *J. Mater. Chem. A* **2018**, 6, 1630.
- [68] W. L. Wu, J. Pu, J. Wang, Z. H. Shen, H. Y. Tang, Z. T. Deng, X. Y. Tao, F. Pan, H. G. Zhang, *Adv. Energy Mater.* **2018**, 8, 1702373.
- [69] H. B. Ding, Q. F. Zhang, Z. M. Liu, J. Wang, R. F. Ma, L. Fan, T. Wang, J. G. Zhao, J. M. Ge, X. L. Lu, X. Z. Yu, B. G. Lu, *Electrochim. Acta* **2018**, 284, 314.
- [70] R. Q. Liu, Z. W. Liu, W. H. Liu, Y. J. Liu, X. J. Lin, Y. Li, P. Li, Z. D. Huang, X. M. Feng, L. S. Yu, D. Wang, Y. W. Ma, W. Huang, *Small* **2019**, 15, 1804533.
- [71] L. Jiao, C. Zhang, C. N. Geng, S. C. Wu, H. Li, W. Lv, Y. Tao, Z. J. Chen, G. M. Zhou, J. Li, G. W. Ling, Y. Wan, Q. H. Yang, *Adv. Energy Mater.* **2019**, 9, 1900219.
- [72] G. L. Chen, W. T. Zhong, Y. S. Li, Q. Deng, X. Ou, Q. C. Pan, X. W. Wang, X. H. Xiong, C. H. Yang, M. L. Liu, *ACS Appl. Mater. Interfaces* **2019**, 11, 5055.
- [73] X. Q. Zhang, W. Yuan, Y. Yang, Y. Chen, Z. H. Tang, C. Wang, Y. H. Yuan, Y. T. Ye, Y. P. Wu, Y. Tang, *Small* **2020**, 16, 2005998.
- [74] S. Y. Zhou, J. Y. Hu, S. G. Liu, J. X. Lin, J. Cheng, T. Mei, X. B. Wang, H. G. Liao, L. Huang, S. G. Sun, *Nano Energy* **2020**, 72, 104680.
- [75] X. L. Zhang, P. Zhang, S. J. Zhang, Y. S. Zhang, R. H. Hou, K. L. Liu, F. J. Miao, G. S. Shao, *J. Energy Chem.* **2020**, 51, 378.
- [76] N. R. Li, L. H. Yu, J. Y. Xi, *Small* **2021**, 17, 2103001.
- [77] H. T. Li, C. Chen, Y. Y. Yan, T. R. Yan, C. Cheng, D. Sun, L. Zhang, *Adv. Mater.* **2021**, 33, 2105067.
- [78] Y. Q. Feng, H. Liu, Y. Liu, F. W. Zhao, J. Q. Li, X. M. He, *J. Energy Chem.* **2021**, 62, 508.
- [79] Z. Li, J. T. Zhang, X. W. Lou, *Angew. Chem., Int. Ed.* **2015**, 54, 12886.
- [80] M. Yan, Y. Zhang, Y. Li, Y. Q. Huo, Y. Yu, C. Wang, J. Jin, L. H. Chen, T. Hasan, B. J. Wang, B. L. Su, *J. Mater. Chem. A* **2016**, 4, 9403.
- [81] Y. Li, D. X. Ye, W. Liu, B. Shi, R. Guo, H. B. Zhao, H. J. Pei, J. Q. Xu, J. Y. Xie, *ACS Appl. Mater. Interfaces* **2016**, 8, 28566.
- [82] Y. Q. Lai, P. Wang, F. R. Qin, M. Xu, J. Li, K. Zhang, Z. Zhang, *Energy Storage Mater.* **2017**, 9, 179.
- [83] Q. Liu, J. H. Zhang, S. A. He, R. J. Zou, C. T. Xu, Z. Cui, X. J. Huang, G. Q. Guan, W. L. Zhang, K. B. Xu, J. Q. Hu, *Small* **2018**, 14, 1703816.
- [84] M. F. Chen, Q. Lu, S. X. Jiang, C. Huang, X. Y. Wang, B. Wu, K. X. Xiang, Y. T. Wu, *Chem. Eng. J.* **2018**, 335, 831.
- [85] N. Wang, S. K. Peng, X. Chen, J. X. Wang, C. Wang, X. Qi, S. L. Dai, S. J. Yan, *RSC Adv.* **2019**, 9, 6346.
- [86] H. Zhang, Q. Qi, P. G. Zhang, W. Zheng, J. Chen, A. G. Zhou, W. B. Tian, W. Zhang, Z. M. Sun, *ACS Appl. Energy Mater.* **2019**, 2, 705.

- [87] H. Chen, W. D. Dong, F. J. Xia, Y. J. Zhang, M. Yan, J. P. Song, W. Zou, Y. Liu, Z. Y. Hu, J. Liu, Y. Li, H. E. Wang, L. H. Chen, B. L. Su, *Chem. Eng. J.* **2020**, *381*, 122746.
- [88] Y. J. Zhang, X. L. Liu, L. Wu, W. D. Dong, F. J. Xia, L. D. Chen, N. Zhou, L. X. Xia, Z. Y. Hu, J. Liu, H. S. H. Mohamed, Y. Li, Y. Zhao, L. H. Chen, B. L. Su, *J. Mater. Chem. A* **2020**, *8*, 2741.
- [89] H. Pan, Z. B. Cheng, X. Zhang, K. Wan, J. Fransaer, J. S. Luo, M. Wubbenhorst, *J. Mater. Chem. A* **2020**, *8*, 21824.
- [90] Z. H. Chen, Y. X. Hu, W. Liu, F. Yu, X. F. Yu, T. Mei, L. Yu, X. B. Wang, *ACS Appl. Mater. Interfaces* **2021**, *13*, 38394.
- [91] J. R. He, L. Luo, Y. F. Chen, A. Manthiram, *Adv. Mater.* **2017**, *29*, 1702707.
- [92] Y. M. Liu, X. Y. Qin, S. Q. Zhang, G. M. Liang, F. Y. Kang, G. H. Chen, B. H. Li, *ACS Appl. Mater. Interfaces* **2018**, *10*, 26264.
- [93] K. Lu, H. Zhang, S. Y. Gao, H. Y. Ma, J. Z. Chen, Y. W. Cheng, *Adv. Funct. Mater.* **2019**, *29*, 1807309.
- [94] Z. Su, M. Q. Chen, Y. K. Pan, Y. J. Liu, H. Xu, Y. Y. Zhang, D. H. Long, *J. Mater. Chem. A* **2020**, *8*, 24117.
- [95] S. S. Xin, J. Li, H. T. Cui, Y. Y. Liu, H. Y. Wei, Y. Y. Zhong, M. R. Wang, *Chem. Eng. J.* **2021**, *410*, 128153.
- [96] Y. G. Zhang, W. L. Qiu, Y. Zhao, Y. Wang, Z. Bakenov, X. Wang, *Chem. Eng. J.* **2019**, *375*, 122055.
- [97] N. X. Shi, B. J. Xi, Z. Y. Feng, F. F. Wu, D. H. Wei, J. Liu, S. L. Xiong, *J. Mater. Chem. A* **2019**, *7*, 4009.
- [98] Z. X. Jian, S. C. Zhang, X. G. Guan, J. J. Li, H. L. Li, W. X. Wang, Y. L. Xing, H. Z. Xu, *RSC Adv.* **2020**, *10*, 32966.
- [99] J. Xu, W. X. Zhang, Y. Chen, H. B. Fan, D. W. Su, G. X. Wang, *J. Mater. Chem. A* **2018**, *6*, 2797.
- [100] R. P. Liu, F. Guo, X. F. Zhang, J. L. Yang, M. Y. Li, M. M. Wu, L. Hang, F. Ming, Z. Lei, *ACS Appl. Energy Mater.* **2019**, *2*, 1348.
- [101] S. Jiao, T. Y. Ding, R. Zhai, Y. P. Wu, S. Chen, W. Wei, *Nanoscale* **2020**, *12*, 13377.
- [102] L. Zhou, H. Li, X. C. Wu, Y. Zhang, D. L. Danilov, R. A. Eichel, P. H. L. Notten, *ACS Appl. Energy Mater.* **2019**, *2*, 8153.
- [103] W. W. Yang, Y. Wei, Q. Chen, S. J. Qin, J. H. Zuo, S. D. Tan, P. B. Zhai, S. Q. Cui, H. W. Wang, C. Q. Jin, J. Xiao, W. Liu, J. X. Shang, Y. J. Gong, *J. Mater. Chem. A* **2020**, *8*, 15816.
- [104] C. Choi, D. Y. Lee, J. B. Park, D. W. Kim, *ACS Sustainable Chem. Eng.* **2020**, *8*, 15134.
- [105] H. X. Wang, B. Zhang, X. Q. Zeng, L. J. Yan, J. C. Zheng, M. Ling, Y. Hou, Y. Y. Lu, C. D. Liang, *J. Power Sources* **2020**, *473*, 228588.
- [106] J. Y. Liu, M. F. Zhu, Z. H. Shen, T. L. Han, T. Si, C. Q. Hu, H. G. Zhang, *Small* **2021**, *17*, 2103051.
- [107] W. L. Wei, J. M. Li, Q. Wang, D. Liu, J. Y. Niu, P. Liu, *ACS Appl. Mater. Interfaces* **2020**, *12*, 6362.
- [108] X. W. Liu, Z. H. Li, X. B. Liao, X. F. Hong, Y. Li, C. Zhou, Y. Zhao, X. Xu, L. Q. Mai, *J. Mater. Chem. A* **2020**, *8*, 12106.
- [109] Y. Guo, Y. Zhang, Y. Zhang, M. W. Xiang, H. Wu, H. K. Liu, S. X. Dou, *J. Mater. Chem. A* **2018**, *6*, 19358.
- [110] F. Wang, X. Ding, R. Y. Shi, M. R. Li, Y. M. Lei, Z. B. Lei, G. S. Jiang, F. Xu, H. Q. Wang, L. C. Jia, R. B. Jiang, Z. H. Liu, J. Sun, *J. Mater. Chem. A* **2019**, *7*, 10494.
- [111] M. W. Xiang, H. Wu, H. Liu, J. Huang, Y. F. Zheng, L. Yang, P. Jing, Y. Zhang, S. X. Dou, H. K. Liu, *Adv. Funct. Mater.* **2017**, *27*, 1702573.
- [112] X. B. Jia, B. S. Liu, J. H. Liu, S. H. Zhang, Z. J. Sun, X. He, H. D. Li, G. F. Wang, H. X. Chang, *RSC Adv.* **2021**, *11*, 10753.
- [113] Y. Q. Tao, Y. J. Wei, Y. Liu, J. T. Wang, W. M. Qiao, L. C. Ling, D. H. Long, *Energy Environ. Sci.* **2016**, *9*, 3230.
- [114] K. Z. Lv, P. F. Wang, C. Wang, Z. H. Shen, Z. D. Lu, H. G. Zhang, M. B. Zheng, P. He, H. S. Zhou, *Small* **2020**, *16*, 2000870.
- [115] F. G. Sun, J. T. Wang, D. H. Long, W. M. Qiao, L. C. Ling, C. X. Lv, R. Cai, *J. Mater. Chem. A* **2013**, *1*, 13283.
- [116] Y. Z. Song, W. Zhao, N. Wei, L. Zhang, F. Ding, Z. F. Liu, J. Y. Sun, *Nano Energy* **2018**, *53*, 432.
- [117] WHO, *inIARC-Evaluation of Carcinogenic Risks to Humans*, International Agency for Research on Cancer, Lyon Cedex, France, **2010**, 193–276.
- [118] M. P. Yu, J. S. Ma, H. Q. Song, A. J. Wang, F. Y. Tian, Y. S. Wang, H. Qiu, R. M. Wang, *Energy Environ. Sci.* **2016**, *9*, 1495.
- [119] M. M. Zhen, K. L. Jiang, S. Q. Guo, B. X. Shen, H. L. Liu, *Nano Res.* **2022**, *15*, 933.
- [120] X. Zhong, I. Rungger, P. Zapol, O. Heinonen, *Phys. Rev. B* **2015**, *91*, 115143.
- [121] Q. Pang, D. Kundu, M. Cuisinier, L. F. Nazar, *Nat. Commun.* **2014**, *5*, 4759.
- [122] X. Y. Tao, J. G. Wang, Z. G. Ying, Q. X. Cai, G. Y. Zheng, Y. P. Gan, H. Huang, Y. Xia, C. Liang, W. K. Zhang, Y. Cui, *Nano Lett.* **2014**, *14*, 5288.
- [123] a) M. T. Liu, S. Jhulki, Z. F. Sun, A. Magasinski, C. Hendrix, G. Yushin, *Nano Energy* **2021**, *79*, 105428; b) S. S. Yao, R. D. Guo, Z. Z. Wu, M. Q. Liu, X. Y. Qian, X. Q. Shen, T. B. Li, L. Wang, Y. H. Wang, S. B. Qin, *J. Electroceram.* **2020**, *44*, 154.
- [124] C. A. Zhou, X. Y. Sun, W. Yan, Y. Z. Zuo, J. J. Zhang, *Chem. - Asian J.* **2022**, *17*, e202200328.
- [125] Y. Liu, J. Wei, Y. X. Tian, S. Q. Yan, *J. Mater. Chem. A* **2015**, *3*, 19000.
- [126] L. B. Ni, Z. Wu, G. J. Zhao, C. Y. Sun, C. Q. Zhou, X. X. Gong, G. W. Diao, *Small* **2017**, *13*, 1603466.
- [127] a) W. Dong, L. Q. Meng, X. D. Hong, S. Z. Liu, D. Shen, Y. K. Xia, S. B. Wang, *Molecules* **2020**, *25*, 1989; b) W. C. Ren, W. Ma, X. Jin, S. F. Zhang, B. T. Tang, *ChemSusChem* **2019**, *12*, 2447.
- [128] a) S. G. Deng, Q. H. Li, Y. H. Chen, C. Wang, H. B. Zhao, J. Q. Xu, J. H. Wu, X. Y. Yao, *Inorg. Chem. Front.* **2021**, *8*, 1771; b) H. Itoh, T. Sugimoto, *J. Colloid Interface Sci.* **2003**, *265*, 283; c) J. Lee, Y. Jeon, J. Oh, M. Kim, L. Y. S. Lee, Y. Piao, *J. Electroanal. Chem.* **2020**, *858*, 113806; d) J. Li, Y. L. Xu, J. P. Wang, *ACS Appl. Energy Mater.* **2021**, *4*, 8368; e) C. Zheng, S. Z. Niu, W. Lv, G. M. Zhou, J. Li, S. X. Fan, Y. Q. Deng, Z. Z. Pan, B. H. Li, F. Y. Kang, Q. H. Yang, *Nano Energy* **2017**, *33*, 306.
- [129] G. X. Liu, K. Feng, H. T. Cui, J. Li, Y. Y. Liu, M. R. Wang, *Chem. Eng. J.* **2020**, *381*, 122652.
- [130] a) X. R. He, Y. J. Zhang, L. F. Yang, J. L. Zhao, H. T. Li, Y. B. Gao, B. Wang, X. D. Guo, *Acta Metall. Sin. (Engl. Lett.)* **2021**, *34*, 410; b) M. Ding, S. Z. Huang, Y. Wang, J. P. Hu, M. E. Pam, S. Fan, Y. M. Shi, Q. Ge, H. Y. Yang, *J. Mater. Chem. A* **2019**, *7*, 25078.
- [131] J. S. Yeon, Y. H. Ko, T. H. Park, H. Park, J. Kim, H. S. Park, *Energy Environ. Mater.* **2022**, *5*, 555.
- [132] a) S. J. M. Rosid, S. Toemen, M. M. A. Iqbal, W. A. W. Abu Bakar, W. N. A. W. Mokhtar, M. M. A. Aziz, *Environ. Sci. Pollut. Res.* **2019**, *26*, 36124; b) C. Z. Yang, R. A. Wong, M. S. Hong, K. Yamanaka, T. Ohta, H. R. Byon, *Nano Lett.* **2016**, *16*, 2969.
- [133] B. Jiang, Y. Qiu, D. Tian, Y. Zhang, X. Q. Song, C. H. Zhao, M. X. Wang, X. Sun, H. H. Huang, C. Y. Zhao, H. Zhou, A. S. Chen, L. S. Fan, N. Q. Zhang, *Adv. Energy Mater.* **2021**, *11*, 2102995.
- [134] H. Cheng, S. C. Zhang, S. Y. Li, C. Gao, S. H. Zhao, Y. Y. Lu, M. Wang, *Small* **2022**, *18*, 2202557.
- [135] Y. Chen, J. Y. Li, X. B. Kong, Y. Y. Zhang, Y. J. Zhang, J. B. Zhao, *ACS Sustainable Chem. Eng.* **2021**, *9*, 10392.
- [136] J. Y. Wang, G. R. Li, D. Luo, Y. G. Zhang, Y. Zhao, G. F. Zhou, L. L. Shui, X. Wang, Z. W. Chen, *Adv. Energy Mater.* **2020**, *10*, 2002076.
- [137] M. H. Li, S. Ji, X. G. Ma, H. Wang, X. Y. Wang, V. Linkov, R. F. Wang, *ACS Appl. Mater. Interfaces* **2022**, *14*, 16310.
- [138] a) G. Pacchioni, *ChemPhysChem* **2003**, *4*, 1041; b) M. V. Ganduglia-Pirovano, A. Hofmann, J. Sauer, *Surf. Sci. Rep.* **2007**, *62*, 219; c) I. Nakamura, N. Negishi, S. Kutsuna, T. Ihara, S. Sugihara, K. Takeuchi, *J. Mol. Catal. A: Chem.* **2000**, *161*, 205; d) J. P. Wang, Z. Y. Wang, B. B. Huang, Y. D. Ma, Y. Y. Liu, X. Y. Qin, X. Y. Zhang, Y. Dai, *ACS Appl. Mater. Interfaces* **2012**, *4*, 4024.

- [139] X. Y. Pan, M. Q. Yang, X. Z. Fu, N. Zhang, Y. J. Xu, *Nanoscale* **2013**, 5, 3601.
- [140] J. W. Wan, W. X. Chen, C. Y. Jia, L. R. Zheng, J. C. Dong, X. S. Zheng, Y. Wang, W. S. Yan, C. Chen, Q. Peng, D. S. Wang, Y. D. Li, *Adv. Mater.* **2018**, 30, 1705369.
- [141] a) J. Wang, D. N. Tafen, J. P. Lewis, Z. L. Hong, A. Manivannan, M. J. Zhi, M. Li, N. Q. Wu, *J. Am. Chem. Soc.* **2009**, 131, 12290; b) D. L. Liu, C. H. Wang, Y. F. Yu, B. H. Zhao, W. C. Wang, Y. H. Du, B. Zhang, *Chem* **2019**, 5, 376.
- [142] L. Sharma, P. Kumar, A. Halder, *ChemElectroChem* **2019**, 6, 3420.
- [143] H. C. Wang, C. Y. Fan, Y. P. Zheng, X. H. Zhang, W. H. Li, S. Y. Liu, H. Z. Sun, J. P. Zhang, L. N. Sun, X. L. Wu, *Chem. - Eur. J.* **2017**, 23, 9666.
- [144] G. M. Wang, Y. Yang, Y. C. Ling, H. Y. Wang, X. H. Lu, Y. C. Pu, J. Z. Zhang, Y. X. Tong, Y. Li, *J. Mater. Chem. A* **2016**, 4, 2849.
- [145] G. C. Xi, S. X. Ouyang, P. Li, J. H. Ye, Q. Ma, N. Su, H. Bai, C. Wang, *Angew. Chem., Int. Ed.* **2012**, 51, 2395.
- [146] C. Y. Fan, C. Chen, J. Wang, X. X. Fu, Z. M. Ren, G. D. Qian, Z. Y. Wang, *Sci. Rep.* **2015**, 5, 11712.
- [147] Y. Y. Zhu, Q. Ling, Y. F. Liu, H. Wang, Y. F. Zhu, *Appl. Catal., B* **2016**, 187, 204.
- [148] a) Y. X. Zhao, Y. F. Zhao, R. Shi, B. Wang, G. I. N. Waterhouse, L. Z. Wu, C. H. Tung, T. R. Zhang, *Adv. Mater.* **2019**, 31, 1806482; b) R. Wu, J. F. Zhang, Y. M. Shi, D. Liu, B. Zhang, *J. Am. Chem. Soc.* **2015**, 137, 6983; c) L. Q. Ye, L. Zan, L. H. Tian, T. Y. Peng, J. J. Zhang, *Chem. Commun.* **2011**, 47, 6951.
- [149] H. B. Lin, S. L. Zhang, T. R. Zhang, H. L. Ye, Q. F. Yao, G. W. Zheng, J. Y. Lee, *Adv. Energy Mater.* **2018**, 8, 1801868.
- [150] H. E. Wang, K. L. Yin, N. Qin, X. Zhao, F. J. Xia, Z. Y. Hu, G. L. Guo, G. Z. Cao, W. J. Zhang, *J. Mater. Chem. A* **2019**, 7, 10346.
- [151] J. W. Wu, Q. Y. Ma, C. Lian, Y. Yuan, D. H. Long, *Chem. Eng. J.* **2019**, 370, 556.
- [152] L. L. Xu, H. Y. Zhao, M. Z. Sun, B. L. Huang, J. W. Wang, J. L. Xia, N. Li, D. D. Yin, M. Luo, F. Luo, Y. P. Du, C. H. Yan, *Angew. Chem., Int. Ed.* **2019**, 58, 11491.
- [153] K. He, T. T. Tsega, X. Liu, J. T. Zai, X. H. Li, X. J. Liu, W. H. Li, N. Ali, X. F. Qian, *Angew. Chem., Int. Ed.* **2019**, 58, 11903.
- [154] Y. J. Li, W. Y. Wang, B. Zhang, L. Fu, M. T. Wan, G. C. Li, Z. Cai, S. B. Tu, X. R. Duan, Z. W. Seh, J. J. Jiang, Y. M. Sun, *Nano Lett.* **2021**, 21, 6656.
- [155] B. Zhang, C. Luo, Y. Q. Deng, Z. J. Huang, G. M. Zhou, W. Lv, Y. B. He, Y. Wan, F. Y. Kang, Q. H. Yang, *Adv. Energy Mater.* **2020**, 10, 2000091.
- [156] Y. P. Gao, L. B. Wang, A. G. Zhou, Z. Y. Li, J. K. Chen, H. Bala, Q. K. Hu, X. X. Cao, *Mater. Lett.* **2015**, 150, 62.
- [157] a) C. F. Zhang, S. J. Kim, M. Ghidui, M. Q. Zhao, M. W. Barsoum, V. Nicolosi, Y. Gogotsi, *Adv. Funct. Mater.* **2016**, 26, 4143; b) C. F. Zhang, M. Beidaghi, M. Naguib, M. R. Lukatskaya, M. Q. Zhao, B. Dyatkin, K. M. Cook, S. J. Kim, B. Eng, X. Xiao, D. H. Long, W. M. Qiao, B. Dunn, Y. Gogotsi, *Chem. Mater.* **2016**, 28, 3937.
- [158] a) Y. P. Lv, S. B. Duan, R. M. Wang, *Prog. Nat. Sci.: Mater. Int.* **2020**, 30, 1; b) M. L. Wang, Y. Z. Song, Z. T. Sun, Y. L. Shao, C. H. Wei, Z. Xia, Z. N. Tian, Z. F. Liu, J. Y. Sun, *ACS Nano* **2019**, 13, 13235.
- [159] D. Q. Cai, J. L. Yang, T. Liu, S. X. Zhao, G. Z. Cao, *Nano Energy* **2021**, 89, 106452.
- [160] X. Wang, D. Luo, J. Y. Wang, Z. H. Sun, G. L. Cui, Y. X. Chen, T. Wang, L. R. Zheng, Y. Zhao, L. L. Shui, G. F. Zhou, K. Kempa, Y. G. Zhang, Z. W. Chen, *Angew. Chem., Int. Ed.* **2021**, 60, 2371.
- [161] a) Y. Z. Song, W. Zhao, L. Kong, L. Zhang, X. Y. Zhu, Y. L. Shao, F. Ding, Q. Zhang, J. Y. Sun, Z. F. Liu, *Energy Environ. Sci.* **2018**, 11, 2620; b) R. P. Fang, S. Y. Zhao, Z. H. Sun, D. W. Wang, R. Amal, S. G. Wang, H. M. Cheng, F. Li, *Energy Storage Mater.* **2018**, 10, 56; c) H. D. Shi, J. Q. Qin, P. F. Lu, C. Dong, J. He, X. J. Chou, P. Das, J. M. Wang, L. Z. Zhang, Z. S. Wu, *Adv. Funct. Mater.* **2021**, 31, 2102314.
- [162] K. Guo, G. Qu, J. Li, H. C. Xia, W. F. Yan, J. W. Fu, P. F. Yuan, J. A. Zhang, *Energy Storage Mater.* **2021**, 36, 496.
- [163] a) K. Xi, D. Q. He, C. Harris, Y. K. Wang, C. Lai, H. L. Li, P. R. Coxon, S. J. Ding, C. Wang, R. V. Kumar, *Adv. Sci.* **2019**, 6, 1800815; b) Y. Q. Mao, W. Sun, X. Y. Yue, W. S. Hou, T. T. Deng, L. L. He, L. Fang, R. Sun, Z. H. Wang, K. N. Sun, *J. Power Sources* **2021**, 506, 230254; c) R. Q. Liu, W. H. Liu, Y. L. Bu, W. W. Yang, C. Wang, C. Priest, Z. W. Liu, Y. Z. Wang, J. Y. Chen, Y. H. Wang, J. Cheng, X. J. Lin, X. M. Feng, G. Wu, Y. W. Ma, W. Huang, *ACS Nano* **2020**, 14, 17308; d) G. Xia, J. J. Ye, Z. Q. Zheng, X. T. Li, C. Z. Chen, C. Hu, *Carbon* **2021**, 172, 96.



Shungui Deng received his Bachelor's and Master's degree from Central South University (China) and Shanghai University (China) in 2018 and 2021, respectively. He used to do research as a jointly trained student at the Ningbo Institute of Material Technology and Engineering, Chinese Academy of Science (NIMTE, CAS) from 2019–2021. Currently, he is a Ph.D. student at École Polytechnique Fédérale de Lausanne (EPFL), Switzerland. He is doing his research at the Swiss Federal Laboratories for Material Science and Technology (Empa) in energy storage and 2D functional materials.



Tiezhu Guo received his Master's degree from South China University of Technology (China) in 2018. He is currently a Ph.D. candidate at Xi'an Jiaotong University (China) and currently stays as a Visiting Ph.D. Student at the Swiss Federal Laboratories for Materials Science and Technology (Empa) in Dübendorf, Switzerland, from 2021–2022. His research interests mainly focus on 2D materials (e.g., MXene, graphene, etc.) for electrochemical energy-related applications.



Jakob Heier is holding a Diploma in Physics from the University of Konstanz (Germany) and a Ph.D. in Materials Science and Engineering from Cornell University (US). Today he is leading a research group at the Swiss Federal Laboratories for Materials Science and Technology (Empa). Activities are ranging from basic studies on 2D materials, practical aspects of large area coating and printing of 2D materials to applications in electronic and photonic devices.



Chuanfang (John) Zhang currently leads a research group at Sichuan University, Chengdu, China focusing on developing functional inks (i.e., MXenes, graphene, and CNFs) for high-precision printing of flexible integrated electronics, including micro-scale energy storage devices, sensors and RFID antennas. He is one of the recipients of the 2022 Clarivate Highly Cited Researcher (cross-field), Rising Stars of Science World 2022 and Top 2% World Leading Scientists issued by Stanford University. He has been elected as Top 10 Leading Chinese Talents in Science and Technology in Europe (2019). His work has been cited 11 200 times with an H-index of 50.